Learning enhances behaviorally relevant representations in apical dendrites

Sam E. Benezra[1,3,4], Kripa B. Patel[2,3,4], Citlali Pérez Campos[2,3,4], Elizabeth M.C. Hillman[1,2,3,4], and Randy M. Bruno[1,3,4,5,6*]

[1] Department of Neuroscience, Columbia University, New York, NY 10027
[2] Departments of Biomedical Engineering and Radiology, Columbia University, New York, NY 10027
[3] Kavli Institute for Brain Science, Columbia University, New York, NY 10027
[4] Zuckerman Mind Brain Behavior Institute, Columbia University, New York, NY 10027
[5] Department of Physiology, Anatomy & Genetics, University of Oxford, Oxford, OX1 3PT

[6] Lead contact

* Correspondence: randy.bruno@dpag.ox.ac.uk (R.M.B.)

SUMMARY

Learning alters cortical representations and improves perception. Apical tuft dendrites in Layer 1, which are unique in their connectivity and biophysical properties, may be a key site of learning-induced plasticity. We used both two-photon and SCAPE microscopy to longitudinally track tuft-wide calcium spikes in apical dendrites of Layer 5 pyramidal neurons as mice learned a tactile behavior. Mice were trained to discriminate two orthogonal directions of whisker stimulation. Reinforcement learning, but not repeated stimulus exposure, enhanced tuft selectivity for both directions equally, even though only one was associated with reward. Selective tufts emerged from initially unresponsive or low-selectivity populations. Animal movement and choice did not account for changes in stimulus selectivity. Enhanced selectivity persisted even after rewards were removed and animals ceased performing the task. We conclude that learning produces long-lasting realignment of apical dendrite tuft responses to behaviorally relevant dimensions of a task.

INTRODUCTION

Learning and memory depend on the ability of biological networks to alter their activity based on past experience. For example, as animals learn the behavioral relevance of stimuli in a sensory discrimination task, neural representations of those stimuli are enhanced[1-7], potentially improving the salience of information relayed to downstream areas. Studies in primary somatosensory (S1)[8] and visual cortex[2] have revealed that top-down signals from distant cortical regions can modify sensory representations during learning, although the cellular and circuit mechanisms underlying this plasticity remain unclear.

Cortical layer 1, comprised mainly of apical tuft dendrites of layer 5 (L5) and layer 2/3 pyramidal neurons, may be a key site driving the enhancement of sensory representations during learning.

Apical tufts are anatomically well positioned for learning, receiving top-down signals from numerous cortical and thalamic areas[9-11]. While L5 distal tufts are electrically remote and far from the soma, they are in close proximity to the highly electrogenic calcium spike initiation zone at the main bifurcation of the apical dendrite, and form a separate biophysical and processing compartment from the proximal dendrites[12-16]. Top-down signals arriving at the tuft can trigger tuft-wide dendritic calcium spikes in L5 neurons[17], which can modulate synaptic plasticity across the entire dendritic tree[18] and potently drive somatic burst firing[15,19-23]. Consistent with this observation, L5 apical dendrite activity is highly correlated with somatic activity[24,25]. Therefore, by strongly influencing somatic activity, L5 apical dendritic calcium spikes can play an important role in modulating cortical output. Several neuromodulators can augment the excitability of the apical tuft and increase the likelihood of eliciting calcium spikes[26,27], which could be a substrate for control of plasticity by behavioral state. Consistent with these ideas, we recently demonstrated that during behavioral training with positive reinforcements, apical tufts in sensory cortex acquire associations that extend beyond their normal sensory modality[28]. In mouse models of dementia and Alzheimer's disease[29,30], tuft dendrites exhibit degeneration which may contribute to the cognitive and memory deficits.

L5 pyramidal neurons are the major source of output from cortex, targeting numerous subcortical structures that affect behavior. The activity of apical dendrites is known to correlate with stimulus intensity, and manipulating L5 apical dendrites and their inputs impacts performance of sensory tasks[17,31-33]. Apical dendritic calcium spikes of pyramidal cells could be a crucial cellular mechanism in learning-related plasticity and behavioral modification[18,34,35]. However, sensory representations of apical tufts, as well as possible changes across learning, have received little attention.

To address this question, we used two-photon microscopy and a new high-speed volumetric imaging technique called Swept Confocally-Aligned Planar Excitation (SCAPE)[36,37] to longitudinally track the activity of GCaMP6f-expressing L5 apical tufts in barrel cortex during a sensory discrimination task. We found that apical tufts underwent extensive dynamic changes in selectivity for task-relevant stimuli as performance improved, even though only one of the stimuli was unrewarded. These changes in responses persisted even after animals disengaged from the task, demonstrating that learning induced long-lasting changes in tuft sensory representations. Animals that were exposed to the same stimulation protocol without any reinforcement did not develop enhanced representations. Our results show for the first time that reinforcement learning expands apical tuft sensory representations along behaviorally relevant dimensions.

RESULTS

Direction discrimination behavior

We devised an awake head-fixed mouse conditioning paradigm that enables controlled investigation of reinforcement effects across learning (Fig.1A,B). In addition to discriminating tactile objects, rodents are known to sense wind direction using their whiskers[38,39] and can be trained to discriminate different directions of whisker deflections[40,41]. With this in mind, we directed brief (100-ms) air puffs at the whiskers in either of two directions: rostrocaudal (backward) or ventrodorsal (upward). One of the directions was paired with a water reward delivered 500 ms after the air puff and thus constituted a conditioned stimulus (CS+). No reward was given for the other direction (CS-).

Licking and whisking were monitored throughout the session (Fig.1C,D). Stimuli elicited a brief passive whisker deflection followed by active whisking over the subsequent ~1.5 seconds (analyzed below, Fig.6). Any anticipatory licks prior to reward delivery were counted as a

78 response. Typically, on the first session, mice exhibited few anticipatory licks to either stimulus
79 (Fig.1C, top, grey shading). By session 2 or 3, mice had learned an association between whisker
80 deflection and reward, but could not discriminate the CS+ and CS- (middle). Within a week (by
81 sessions 7-9), every mouse we tested learned to reliably lick to the CS+ while withholding licks
82 to the CS-, performing substantially above chance after a single week of training (Fig.1C, bottom;
83 Fig.1E,F). Thus, mice rapidly learned to discriminate the direction of whisker stimuli in our
84 behavioral task.
85
86 **Overall stimulus-evoked activity is unbiased and stable across conditioning**
87 To investigate the effects of reinforcement learning on apical tuft activity, we imaged apical tufts
88 (433 x 433 μm field of view) across conditioning days as well as on an unrewarded pre-
89 conditioning day to measure naïve stimulus responses and an unrewarded post-conditioning day
90 to detect any long-lasting changes in responses (Fig.1B). We virally delivered the gene for Cre-
91 dependent GCaMP6f[42] in the barrel cortex of Rbp4-Cre mice, which labels a heterogeneous
92 population of pyramidal neurons comprising approximately 50% of layer 5[28,43,44]. By targeting
93 our injections to layer 5B, we predominantly labeled thick-tufted pyramidal neurons (see
94 Methods). Using intrinsic signal imaging, we mapped the location of the C2, D2, and gamma
95 whisker barrel columns and identified an overlapping region in layer 1 with sufficient GCaMP6f
96 expression (Fig.2A). The air puff nozzles were aimed toward the whiskers corresponding to this
97 region. Dendritic activity was longitudinally recorded from the same field-of-view (horizontal
98 location and depth) in layer 1 across all sessions (Supplementary Movie 1).
99
100 To extract calcium signals from individual cells, we segmented tufts using CaImAn, a sparse non-
101 negative matrix factorization method that clusters pixels according to their temporal correlation[45]
102 (see Methods), and analyzed regions of interest exhibiting apical tuft structure (Fig.2B; 65 ± 15
103 tufts per mouse; mean ± SD). Individual segmented tufts were substantial in their spatial extent

104 (>100 μm), reflecting tuft-wide voltage-gated calcium spikes rather than branch-specific N-
105 methyl-D-aspartate (NMDA) receptor-mediated spikes. All calcium analyses hereafter refer to
106 tuft-wide calcium spikes. Average responses to an event include failures. In many tufts, the CS+
107 and CS- reliably evoked an influx of calcium that robustly activated the tuft (e.g. Fig.2C).
108 Successful calcium events across tufts averaged 28% ΔF/F, consistent with previous studies of
109 layer 5 apical dendrites[17,31]. Interestingly, during intermediate but not early learning, the average
110 population response to the CS+ exhibited a two-peak structure (Supp Fig.1, session 4) similar to
111 tuft reward-related signals we observed previously in barrel cortex[28]. By the last-rewarded and
112 post sessions, the second CS+ peak was no longer visible, which could be an endpoint of mice
113 learning that the conditioned stimulus predicts the upcoming reward.
114
115 Reward can alter somatic receptive fields in the auditory, visual, and somatosensory cortex of
116 both rodents and non-human primates such that rewarded stimulus representations become more
117 robust after learning[4,5,28,46], although cortical sensory responses can remain unchanged during
118 learning[47]. We investigated whether calcium responses to the CS+ increased in the tuft population
119 as animals learned its association with reward (Fig.2). Average responses of tufts to the CS+ and
120 CS- were similar during the pre-conditioning session (Fig.2D; $p = 0.20$, signed rank test, $n = 440$
121 pre tufts and 418 post tufts), indicating that there was no inherent bias in the population toward a
122 particular stimulus in naïve animals. Surprisingly, even after learning, responses to the CS+ and
123 CS- were similar on the last- and post-conditioning sessions ($p = 0.62$, 0.64, respectively, signed
124 rank test), revealing that no bias develops for the CS+ among dendritic tufts. Only a minority of
125 tufts exhibited statistically significant average responses to air puff stimuli (CS+ responsive: 26 ±
126 8%; CS- responsive: 25 ± 8%; mean ± SD across all sessions). When we excluded responses that
127 were not statistically significant (see Methods), we again found no difference between the
128 average response amplitudes to the CS+ and CS- on the pre, last-rewarded, and post sessions ($p =$
129 0.65, 0.31, and 0.69, respectively, rank sum test; data not shown). Similarly, the probability of

transients in response to CS+ versus CS- (see Methods) did not differ during pre-conditioning ($p = 0.66$) or post-conditioning sessions ($p = 0.44$). Therefore, reinforcement learning in our paradigm does not bias tuft representations toward the rewarded stimulus.

While a bias for the CS+ did not develop after learning, we wondered whether overall tuft responses to both conditioned stimuli increased as animals learned the task. Linear regression analysis revealed that conditioning session number was a poor predictor of both CS+ and CS- amplitudes (All tufts R^2, CS+: 0.0064, CS-: 0.0035, Fig.2E; Significantly responding tufts R^2, CS+: 0.014, CS-: 0.014, data not shown). We did find a small but significant decrease in amplitude from pre to last for CS+ ($p < 0.01$) and CS- ($p < 10^{-7}$), but this was not permanent: amplitudes did not significantly differ between the pre and post sessions (Fig.2D; $p = 0.53$, 0.33, CS+ and CS- respectively, Wilcoxon rank sum test). Taken together, these findings demonstrate that reinforcement learning does not robustly bias the magnitudes of tuft calcium responses to either stimulus at the population level.

Development of tuft selectivity with task learning

While learning produced no bias in overall tuft activity, learning might enhance selectivity for conditioned stimuli. Barrel cortex neurons are tuned to the angle of whisker deflection[48-50], indicating that the sets of synaptic connections activated by the CS+ and CS- may be overlapping but should not be identical. Therefore, the possibility exists that responses to the CS+ and CS- can change independently of each other. To examine this, we compared the amplitude of the average response to CS+ and CS- trials for all segmented tufts on the pre, last-rewarded, and post sessions (Fig.3A; n = 7 mice; 465 pre, 442 last-rewarded, and 430 post tufts). In agreement with our previous analysis, we found no significant bias toward CS+ or CS- during any of the three sessions (Pre: $p = 0.20$; last-rewarded: $p = 0.43$; Post: $p = 0.64$, sign-rank test). Under naïve conditions during the pre session, most tufts that responded to air puff stimuli did not strongly

156 prefer the CS+ or CS- (Fig.3A, left). Surprisingly, on the last-rewarded session and the
157 unrewarded post-conditioning session, we observed a prominent shift in the response distribution,
158 where many tufts exhibited more selective responses to one stimulus or the other (Fig.3A, middle
159 and right).
160
161 Plasticity can occur after repeated exposure to stimuli even in the absence of reinforcements[51-55].
162 To test whether enhanced selectivity depended on reinforcement, we imaged a separate group of
163 similarly water-restricted mice that were repeatedly exposed to the same stimuli for the same
164 number of days but without any reward. Repeated exposure mice exhibited a stable distribution of
165 response selectivity over time (Fig.3B; a separate cohort of 7 mice; 317, 313, and 321 tufts on
166 Day 1, Day 8, and Day 9, respectively). These results suggest that reinforcement learning, and not
167 simply repeated stimulus exposure, drives apical tufts to become more selective for either the
168 CS+ or CS-.
169
170 To directly quantify the response selectivity of tufts, we computed a selectivity index (SI; see
171 Methods) ranging from -1 (exclusively CS- responsive) to 1 (exclusively CS+ responsive) for
172 each tuft. Initially in both the conditioned and repeated exposure mice, the SI distribution was
173 centered around zero, indicating that most tufts in naïve animals did not strongly prefer either
174 stimulus (Fig.3C,D, left panels). Consistent with our other analyses (Fig.2D), the mean SI
175 remained close to zero for each of the three sessions (-0.049, -0.001, and 0.003 for pre-
176 conditioning, last rewarded, and post-conditioning days, respectively), confirming that learning
177 produced no overall bias toward one particular stimulus among the population. During learning,
178 the SI distribution of conditioned but not repeated exposure mice shifted markedly, whereby a
179 much greater proportion of neurons were highly selective for either the CS+ or CS- (Fig.3C,D,
180 middle and right panels, |SI| pre versus last-rewarded: $p < 10^{-6}$, |SI| pre versus post: $p < 10^{-5}$;
181 Wilcoxon rank sum test). These effects can even be observed within individual mice, with

learning significantly increasing tuft selectivity in individual conditioned mice, but not repeated exposure mice (Supp.Fig.2). The degree of enhancement in tuft selectivity was closely correlated with conditioned animals' ability to discriminate stimuli across sessions (Fig.3E; Pearson's R = 0.60, $p < 10^{-5}$).

Whereas selectivity magnitude (|SI|) only considers the amplitude of tuft responses to CS+ and CS-, their discriminability also depends on their variability. For example, a large difference in CS+ and CS- responses would not be discriminable if the variability of those responses were very high; a small difference might be discriminable if the variability were low. We therefore additionally calculated a d-prime metric of neural discriminability that normalizes differences in response magnitudes to each stimulus by their variability (see Methods). In conditioned animals, neural discriminability of CS+ and CS- responses of tufts increased significantly across learning (Fig.3F, blue; first-rewarded versus last-rewarded: $p < 10^{-3}$, pre versus post: $p < 10^{-4}$; Wilcoxon rank sum test). By contrast, neural discriminability of tuft responses in the repeated exposure mice decreased slightly with progressive exposure to the stimuli (Fig.3F, gray; Day 1 versus Final: $p < 0.01$). Taken together, these results show that enhanced stimulus representations can emerge in apical tufts, but require reinforcement.

The above analyses rely on the accurate measurement of calcium spikes from individual tufts. While two-photon microscopy acquires images with high resolution and speed, the imaging field is restricted to a single focal plane. This method can only measure calcium signals from a thin cross-section of the three-dimensionally complex apical structures. Indeed, many of the spatial components extracted from our two-photon data were comprised of dendritic branches that cross the imaging plane at different locations (Supp.Fig.3A), which makes it difficult to determine whether the segmentation software accurately extracted signals from one tuft or erroneously merged multiple tufts. For the same reasons, a single apical tuft could be falsely classified as two

208 different tufts. Such errors could mislead our interpretation of selectivity in the population,
209 especially given that a single apical tuft can exhibit non-homogenous branch-specific
210 events[15,56,57].
211
212 To confirm that our interpretation was not due to segmentation errors, we repeated the
213 conditioning experiment using a new, high-speed volumetric imaging approach called
214 SCAPE[36,37], which allowed us to monitor calcium across entire apical tufts (Supplementary
215 Movie 2). These three-dimensional datasets (300 × 1050 × 234 μm field of view) encompassed
216 large portions of the apical tree which included branches converging on their bifurcation points in
217 layer 2, enabling us to identify whole apical trees unambiguously (Fig.4A,B; Supp.Fig.3B).
218 CaImAn effectively demixed overlapping trees in these three-dimensional volumes. SCAPE
219 microscopy, we imaged tuft activity of additional mice conditioned with the same behavioral
220 paradigm (Fig.4C). Comparison of tuft responses to the CS+ and CS- on the pre, last-rewarded,
221 and post sessions (Fig.4D; 241 pre, 215 last-rewarded, 150 post tufts in 2 mice) revealed again
222 that task learning induced significant increases in tuft selectivity (Fig.4E; pre versus last-
223 rewarded: $p < 10^{-5}$, pre versus post: $p < 10^{-4}$, Wilcoxon rank sum test of |SI|). On average, the SI
224 magnitudes were similar between tufts imaged using 2-photon microscopy and SCAPE (mean ±
225 s.e.m. |SI| for 2-photon versus SCAPE; pre: 0.41±0.01 versus 0.40±0.02; last-rewarded:
226 0.54±0.02 versus 0.54±0.02; post: 0.51±0.02 versus 0.53±0.03). These data demonstrate that the
227 effects in our two-photon dataset are not caused by errors in segmentation, but rather reflect
228 changes at the level of individual dendritic tufts. Our results, based on two different imaging
229 approaches, clearly demonstrate that reinforcement increases stimulus selectivity at the level of
230 the entire apical tuft.
231
232 **Selective tufts emerge from both initially unresponsive and responsive populations**

The striking effect of reinforcement learning on tuft response selectivity could develop in several ways. For example, initially unresponsive tufts could develop a robust response to either stimulus after learning (e.g., Fig.5A, top). Conceivably, tufts that were initially unselective in naïve animals could also maintain their response to one stimulus while losing their response to the other (e.g., Fig.5A, middle). Either or both scenarios could lead to the increase in neurons that are selective for stimulus direction. To investigate which changes in individual tufts underlie population-wide improvements in stimulus selectivity, we longitudinally tracked the same set of tufts across all sessions and compared their selectivity in pre- and post-conditioning sessions for both conditioned and repeated exposure mice.

First, we categorized tufts that were unresponsive to either stimulus on the first imaging session, which accounted for the large majority of tufts (conditioned: 458/603; repeated exposure: 334/457), and compared their response to the CS+ and CS- on the last session to determine if they became selective (Fig.5B, see Methods). Stimulus-unresponsive tufts, while on average less active than responsive ones (median calcium events per minute: 2.65 versus 3.66 for stimulus-unresponsive and responsive tufts, respectively; $p < 10^{-40}$, Wilcoxon rank sum test; Supplementary Fig.4), were not silent, with many undergoing tuft-wide calcium influx several times per minute. Silent tufts that are never active during the session may not have been detected in our imaging, but we were able to detect tufts that discharged as few as 3 voltage-gated calcium spikes over a 30-minute behavioral session. Interestingly, in both the conditioned and repeated exposure mice, approximately 40% of initially unresponsive tufts developed a response to at least one stimulus by the last session, becoming either selective or unselective (Fig.5B). However, in conditioned animals, the proportion of initially unresponsive tufts that became selective was significantly larger than in repeated exposure mice ($p = 0.04$, 2-sample t-test comparing mice). Furthermore, while the proportion of selective and unselective tufts in this category was similar

258 for conditioned animals, unselective tufts were more common in repeated exposure mice ($p =$
259 0.03, paired t-test).
260
261 Next, we analyzed tufts that were initially responsive and either selective (Fig.5C; conditioned:
262 56/603, RE: 43/457) or unselective (Fig.5D; conditioned: 89/603, repeated exposure: 80/457). In
263 these smaller categories, we found no significant differences in the outcome of selectivity
264 between the two groups of animals. Together, these results indicate that, while both stimulus
265 exposure and reinforcement can alter tuft tuning, the presence of reward increases the likelihood
266 that initially unresponsive tufts develop selectivity for either the CS+ or CS- (summarized in
267 Fig.5E).
268
269 While a greater proportion of tufts from the conditioned animals were selective during the final
270 session (20.2% versus 10.3% of tufts from conditioned and repeated exposure mice, respectively),
271 we wondered whether conditioning also impacted the degree of selectivity. Note that some tufts
272 had very small yet statistically different CS+ and CS- response amplitudes and were thus
273 classified as selective despite a small SI. First, we compared the SI of initially unresponsive tufts
274 on the final imaging session (Fig. 5F). Supporting our results in Fig. 5B, the SI distribution was
275 shifted toward the tails in conditioned, but not repeated exposure mice, indicating that reward
276 enhances selectivity for either the CS+ or CS- in this subset (|SI| conditioned versus repeated
277 exposure: $p < 10^{-5}$, Wilcoxon rank sum test, $n = 199$ and 110 tufts, respectively).
278
279 Next, we compared the |SI| of all tufts that were categorized as selective during the last imaging
280 session in conditioned and repeated exposure mice (Fig. 5G). Interestingly, we found that even
281 among selective tufts, the |SI| distribution in conditioned mice was significantly greater than in
282 repeated exposure mice ($p = 0.006$, Wilcoxon rank sum test, $n = 122$ and 47 tufts, respectively),

283 indicating that while selective tufts are present after both conditioning and repeated stimulus
284 exposure, the magnitude of selectivity is stronger after conditioning.
285
286 We then quantified the change in |SI| of all tufts that were responsive in both the first and last
287 sessions by computing the difference between the two sessions (Fig. 5H). Tufts in conditioned
288 mice exhibited a greater increase in |SI| across sessions compared to repeated exposure mice ($p =$
289 0.01, Wilcoxon rank sum test, $n = 48$ and 42 tufts, respectively), demonstrating that the
290 magnitude of selectivity in initially responsive tufts increases after reinforcement learning.
291
292 Finally, we found that the degree of selectivity of tufts that eventually became unresponsive on
293 the last session was overall similar between the two groups (Fig.5I, |SI| conditioned versus
294 repeated exposure: $p = 0.06$, Wilcoxon rank sum test, $n = 97$ and 81 tufts, respectively). However,
295 tufts that became unresponsive were more likely to be initially highly selective in the conditioned
296 group than in the repeated exposure group (19 tufts with initial $|SI| > 0.75$ / 97 tufts ending as
297 unresponsive in the conditioned group versus 3/81 in the repeated exposure group; $p = 0.0013$, Z
298 approximation to binomial). Therefore, learning can involve a loss of responsivity in a small
299 subset of well-tuned tufts.
300
301 In summary, our longitudinal analyses revealed that reinforcement learning biases initially
302 unresponsive tufts toward becoming selective and enhances the selectivity of tufts that are
303 initially responsive.
304
305 **Neither movement nor behavioral choice account for enhanced selectivity**
306 Several plausible factors could underlie the changes in selectivity we observed across learning.
307 For instance, movements like whisking are correlated with layer 5 somatic action potentials[58-60]
308 and might have impacted calcium activity in the apical tuft. To investigate whether whisking

309 could account for the changes in tuft selectivity, we imaged the whiskers with a high-speed
310 camera and computed whisking amplitude (see Methods) while mice underwent conditioning and
311 two-photon imaging (Fig.6A). First, we considered whether animals changed their whisker
312 movements in response to conditioned stimuli over the course of learning. We computed the peak
313 of the mean stimulus-aligned whisking amplitude for the CS+ and CS- (Fig.1C, left; Fig.6B) for
314 each session in five mice. Although conditioning alters licking behavior (Fig.1C,E), the
315 magnitudes of whisker movements following both stimuli were stable across sessions (Fig.6B;
316 CS+: $p = 0.44$; CS-: $p = 0.45$; linear regression). We also computed the standard deviation (SD)
317 of stimulus-evoked whisker amplitude across trials for all sessions (Fig. 6C). While the whisking
318 amplitude became slightly more reliable (decreased SD) across sessions ($p < 10^{-4}$), the change in
319 reliability across sessions was similar for CS+ and CS- ($p = 0.53$). Therefore, whisking is similar
320 on both trial types throughout learning.
321
322 We next examined whether whisking was correlated with tuft calcium activity by comparing
323 stimulus-triggered averages and intertrial interval (ITI) whisk-triggered averages of all tufts
324 during post-conditioning. Whisking amplitude was similar between spontaneous ITI whisking
325 bouts and evoked whisking responses to stimuli ($n = 115$ and 617 events, respectively; $p = 0.53$,
326 Wilcoxon rank sum test). In contrast to air puff stimuli, ITI whisking bouts were not associated
327 with a robust calcium response (Fig.6D).
328
329 To quantify the relationship of whisking and sensory stimuli to tuft calcium spikes, we performed
330 a linear regression analysis (see Methods) on 322 tufts using calcium influx as the response
331 variable and either stimulus or whisking amplitude as a single predictor variable (Fig.6E). Air
332 puff stimuli more reliably predicted calcium influx than whisking amplitude for each of virtually
333 all tufts ($p < 10^{-12}$, sign rank test). These results are consistent with other studies that found either
334 only weak or no correlation between whisking and L5 tuft calcium spikes in S1[28,31,32].

335 Furthermore, we found no relationship between the whisking response and the median SI
336 magnitude on a given session (Fig.6F, whisking to CS+ $p = 0.22$, CS- $p = 0.78$). Therefore,
337 changes in whisker movement cannot account for the changes in selectivity during learning that
338 we observed.
339
340 Finally, the possibility remains that other task-related signals relaying information about reward
341 expectation and behavioral choice could impact apical tuft activity and drive increases in
342 selectivity. To test this, we compared tuft responses to the CS- in false alarm trials (FA; mouse
343 incorrectly licked for reward) and correct rejection trials (CR; mouse correctly withheld licks) to
344 determine if their activity was modulated by behavioral choice. Notice that these two trial types
345 have the same sensory input but involve different choices. (The corresponding analysis for CS+
346 trials is not technically possible for lack of sufficient Miss trials after the first conditioning day,
347 an issue also observed in[1].) Tufts were classified as behaviorally modulated if the FA response
348 was significantly different from the CR response, and were not behaviorally modulated if CR and
349 FA responses were statistically indistinguishable (e.g. Fig.7A). Behaviorally modulated tufts
350 accounted for only ~10% of the total tuft population in both early and late learning (50/395 in
351 early; 35/406 in late learning).
352
353 To test whether these behaviorally modulated tufts contributed to increased selectivity during
354 learning, we excluded them and compared selectivity of the remaining behaviorally-insensitive
355 tufts. We found that selectivity increased significantly from early to late learning (Fig.7B,C;
356 median |SI| of 345 tufts early versus 371 tufts late learning: 0.38 versus 0.47, $p = 0.02$, Wilcoxon
357 rank sum test), similar to our previous analysis of the entire population. Licking, like whisking,
358 was a relatively poor predictor of tuft calcium influx (Supp.Fig.5A,B). Because some
359 behaviorally modulated tufts may not have been statistically detectable, we used multivariate
360 linear regression to disentangle stimulus responses from licking and whisking, which may have

been confounded with choice. Median coefficients for licking and whisking were on average 3.3 times smaller than median stimulus coefficients for the first rewarded, last rewarded, and post sessions (all $p < 10^{-6}$, Wilcoxon rank sum test). Even after we factored out possible effects of movements, CS+ and CS- coefficients were enhanced by learning but not repeated exposure (Supp.Fig.5C,D), consistent with our other analyses. Together, these results demonstrate that enhanced selectivity during learning cannot be explained by non-sensory signals related to the animals' behavior.

Enhanced selectivity in barrel cortex is long-lasting when mice exclusively use whiskers

Mice could conceivably exploit other sensory cues to learn and perform the task, such as auditory cues from the air nozzles or non-whisker tactile cues from air current eddies contacting the fur or skin. To determine which mice exclusively used their whiskers to distinguish the CS+ and CS-, we trimmed all whiskers after the post-conditioning session and assessed performance in five mice. Performance in each of the five mice decreased after whisker trimming, indicating that each used some whisker information. Three mice performed the task exclusively with their whiskers, falling to chance levels after the whisker trim ("whiskers only"). Two other mice still performed the task above chance after the whisker trim, indicating that they were not exclusively using their whiskers and exploited information from multiple sensory streams ("whiskers + other senses").

We examined whether these two different behavioral strategies impacted tuft selectivity. Both the "whiskers only" and "whiskers + other senses" groups exhibited enhanced tuft selectivity in the last-rewarded session relative to pre-conditioning. This effect was more pronounced in the "whiskers only" mice (Fig.8A,B, left and middle; whiskers only: median |SI| of 180 pre tufts versus 169 last-rewarded tufts: 0.36 versus 0.59, $p < 10^{-3}$; "whiskers + other senses": median |SI| of 144 pre tufts versus 155 last-rewarded tufts: 0.39 versus 0.50, $p = 0.01$). Surprisingly, enhanced selectivity persisted during the post-conditioning session for the "whiskers only" group

but not the “whiskers + other senses” group (Fig.8A,B right panels; whiskers only: median |SI| of pre versus 167 tufts post: 0.36 versus 0.58; $p < 10^{-3}$; whiskers + other senses: median |SI| of 155 pre versus post tufts: 0.39 versus 0.42; $p = 0.45$). Therefore, tuft selectivity in barrel cortex is enhanced regardless of behavioral strategy, but outlasts conditioning only when mice rely solely on their whiskers to perform the task.

We further examined this persistence of enhanced tuft selectivity as experienced mice stopped performing the task. While the entire post-conditioning session was unrewarded, mice initially expected rewards and licked for many CS+ trials in the first half of the session. By the second half of the session, the probability of a lick occurring during the CS+ extinguished, approaching zero (Fig.8C). We compared the selectivity of tufts during the first and second halves of the post-conditioning sessions of mice that exclusively used their whiskers and found no difference in the two distributions (Fig.8D, $p = 0.94$, Wilcoxon rank sum test of |SI|), demonstrating that selectivity of the population remained stable throughout the session. Taken together, these results demonstrate that enhanced stimulus selectivity of apical tuft dendrites after reinforcement learning is long lasting, persisting even after mice cease performing the task and expecting reward.

DISCUSSION

Our study is the first to investigate how learning a discrimination task alters apical tuft activity. Using both novel volumetric whole-tuft imaging and conventional planar microscopy, we discovered that L5 apical tufts acquire enhanced representations of multiple stimuli during learning. Rather than simply retuning tufts toward the rewarded stimulus, learning enhanced selectivity for both stimuli, suggesting that tufts are aligning themselves to the behaviorally relevant stimulus dimensions. These enhanced sensory representations persist even after mice

413 cease performing the task. In contrast, representations are slightly degraded by mere repeated
414 exposure to stimuli outside of a task. Consistent with previous studies[28,31], we found that
415 movement in and of itself has little direct impact on tuft spikes, indicating that increased
416 selectivity of apicals reflects alterations in sensory coding as animals learn. This sensitization of
417 tufts to behaviorally relevant sensory dimensions may be a general feature of all sensory cortical
418 areas.
419
420 Tuft spikes enhance plasticity of synaptic inputs that occur over behavioral (seconds-long)
421 timescales[18,34]. These new behaviorally relevant tuft representations may therefore prime
422 subsequent plasticity of synapses across the entire pyramidal neuron. Additionally, tuft events
423 potently modulate somatic burst firing and enhance how somata respond to their basal inputs[15,61].
424 As learning and plasticity increase apical selectivity for a behaviorally relevant axis, tuft events
425 will unavoidably amplify somatic burst output along the same axis. This could enable action
426 potential output of L5 cells in primary sensory cortex to directly drive behavioral responses via
427 projections to movement related areas, such as the corticostriatal, corticopontine, and
428 corticotrigeminal pathways. Thus, tuft spikes have the potential to modify somatic output, both in
429 the present and in the future.
430
431 **Enhanced Representation of Behaviorally Relevant Stimuli**
432
433 Enhancing the representation of relevant stimulus dimensions rather than a singularly important
434 stimulus, such as a rewarded event, has multiple benefits for behavior. In our paradigm, both the
435 CS+ and CS- are predictive of whether or not a reward will occur in the future. Explicitly
436 encoding both stimuli could allow sensory cortical areas to directly elicit actions. In the context of
437 this task, CS+ preferring tufts in barrel cortex may trigger anticipatory licking while CS-
438 preferring tufts could suppress licking. L5 cells in sensory cortex via their output to striatum,

pons, brain stem, and spinal cord would thereby be able to directly and rapidly drive action without further cortical processing, such as by frontal areas including motor cortex[32,62]. Such rapid sensory-motor transformations by primary sensory areas may be critical for natural time-constrained behavior.

Furthermore, learning produced a representation in which the degree of selectivity for the two stimuli was continuous and uniformly distributed. Exclusively CS+ or CS- selective apicals never dominated the population. Continuous degrees of selectivity across the population, rather than discrete representations, may allow the system to be more robust to the variability caused by active movements that alter sensory input. A continuous distribution may also facilitate future adjustments of neural representations as subjects continue to learn a task or encounter new tasks. The uniformity we observed may reflect that neurons are high-dimensional, being sensitive to mixtures of variables[60,63-65], only one of which might be altered here by learning. The uniform distribution of selectivity corresponds to a full range of pessimism to optimism concerning stimulus predictions of upcoming rewards. Recent work shows that behavioral performance benefits from reinforcement learning that incorporates the distribution of reward probabilities rather than just the average expected reward value[66]. L5 corticostriatal synapses could theoretically afford a plastic substrate for acquiring the necessary distribution of reward probabilities.

Surprisingly, past studies in which mice were trained to associate one or more stimuli with a reward typically show that cortical representations are stronger for the rewarded stimulus [1,3,5]. In contrast to these studies of layer 2/3 somatic activity, our experiments revealed that the overall tuft calcium response to the CS+ and CS- at the population level did not change significantly after animals learned the task (Fig.2). Instead, representations for both stimuli were enhanced by individual tufts developing selectivity for either the CS+ or the CS- (Fig.3). This divergence in

465 phenomena may result from several important differences between our work and the
466 aforementioned studies.
467
468 First, enhanced selectivity for both rewarded and unrewarded stimuli could be a phenomenon that
469 is unique to the apical dendritic tufts. In addition to local inputs, the apical tufts of pyramidal cells
470 in S1 receive long-range top-down input from several sources, including motor cortex[31,67],
471 secondary somatosensory cortex[11], and secondary thalamus[9,10,68]. Frontal areas, such as prefrontal
472 cortex, indeed have enhanced representations of the CS+ and CS- after learning[47]. In contrast,
473 input to the somata is dominated by the local cortical area and primary thalamus[69,70]. While
474 somato-dendritic coupling can be strong in L5 neurons[25], it is asymmetric; at least 40% of
475 somatic transients attenuate in a distance-dependent manner along the apical trunk and distal
476 tufts[24]. The non-overlapping anatomical inputs and asymmetric coupling together could produce
477 different learning-related effects on apical tuft and somatic stimulus representations.
478
479 Second, learning-related changes may manifest differently in layer 2/3, the usual focus of
480 previous studies[1,3], and layer 5 pyramidal cells, the tufts of which we studied. With the exception
481 of a small population of corticostriatal cells, most excitatory cells in layer 2/3 project to other
482 cortical areas to affect further cortical processing[71,72]. In contrast, many L5 cells project to
483 subcortical structures including the thalamus, superior colliculus, and brainstem, which may
484 directly trigger behavioral responses[73-75]. In discrimination paradigms, both stimuli are relevant to
485 behavior. In our task, the CS+ prompted licking to obtain a reward, and the CS- suppressed
486 licking that would have no benefit. Thus, an enhanced representation of both stimuli in layer 5
487 would be advantageous for animals to perform the task efficiently. Recently, it was shown that
488 apical dendrite activation of subcortical-targeting pyramidal tract L5 cells, but not
489 intratelencephalic L5 cells that are more like L2/3 cells in their connectivity, determines the
490 detection of tactile stimuli[32]. The Rbp4-Cre mice we used in this study labels a heterogenous

population of layer 5 pyramidal cells, comprising both pyramidal tract and intratelencephalic neurons. In the future, it would be interesting to examine whether learning has different effects on the sensory representations of these two populations. Moreover, direct comparisons of the layers would be particularly informative.

Candidate Plasticity Mechanisms

Enhanced selectivity could be due to changes in local synaptic connectivity, long-range inputs, or both. Learning may strengthen and weaken synapses onto barrel cortex neurons from ascending thalamocortical input or from neighboring cells. Such local plasticity could enhance CS+ or CS- responsiveness. Alternatively or additionally, other cortical regions encoding task context could via long-range inputs reconfigure barrel cortex to respond more strongly to these stimuli. The present results do not completely distinguish between these two scenarios because long-range inputs may still encode the context while the mouse is in the behavioral apparatus. However, we found that enhanced representations persist after mice are no longer engaged in the task and receiving rewards. This result suggests that enhanced representations may be a product of local plasticity in sensory cortex that alters receptive fields.

Even in the absence of reward, repeated exposure to stimuli can drive plasticity in sensory cortex and alter response tuning. For instance, repeated exposure to oriented gratings can alter the orientation tuning of cells in primary visual cortex[51-53], and overstimulation of whiskers induces plasticity at dendritic spines and alters whisker representations in somatosensory cortex[54,76]. Our results demonstrate that at the population level enhanced representations developed only when stimuli were behaviorally relevant. Our longitudinal analysis revealed that while the response dynamics of some tufts changed after repeated stimuli presentations, overall selectivity of the population did not increase when rewards were omitted (Figs.3&5). This raises the question: What are the mechanisms that drive enhanced selectivity under rewarded conditions? In one

517 possible scenario, reward delivery causes the release of neuromodulators that augment the
518 activity of apical tufts. Cortical layer 1 is innervated by cholinergic afferents from the nucleus
519 basalis[77] and adrenergic afferents from the locus coeruleus[78], the main source of acetylcholine and
520 norepinephrine, respectively. Salient events such as reward and arousal lead to the release of
521 these neuromodulators in cortex[79,80], which could increase the excitability of apical dendrites by
522 recruiting disinhibitory circuits or directly influencing dendritic currents[26,27,79,81]. In this model,
523 the release of reward-driven neuromodulators promotes plasticity and an enhanced representation
524 of temporally aligned sensory inputs. This phenomenon was demonstrated in auditory cortex,
525 where tones paired with stimulation of the nucleus basalis shifted the tuning of neurons toward
526 the frequency of the paired stimulus[82].
527
528 Why are representations of the CS- equally enhanced when there is no associated reward? One
529 explanation is that, as mice learn that the CS- indicates absence of reward, the CS- effectively
530 signals punishment and acquires negative value. Acetylcholine is released in response to aversive
531 stimuli, and can activate disinhibitory microcircuits that reduce inhibition onto pyramidal cells
532 and may be essential for learning[83,84]. Thus, it is possible that both the CS+ and CS-
533 representations are enhanced by neuromodulatory mechanisms tied to reward and punishment,
534 respectively. An open question is whether the outcome is due to reinforcement learning or the
535 behavioral state brought on by the reinforcers rather than their valence. Sensory cortical plasticity
536 may not be tied to reinforcer valence. Our paradigm creates an environment where mice benefit
537 from being attentive and engaged in order to maximize reward while minimizing effort. Previous
538 work has shown that active engagement in a visual discrimination task was associated with
539 significantly higher selectivity in layer 2/3 cells in visual cortex[1]. Task engagement may lead to a
540 sustained increase in neuromodulator release throughout the conditioning session, priming the
541 apical dendrites for plasticity and the development of selective responses for task-relevant stimuli
542 as they learn.

543

544 What determines whether a particular tuft eventually becomes selective for the CS+ or CS-? Our
545 longitudinal analysis revealed that many tufts that were initially unresponsive to either stimulus
546 developed a highly selective response to either the CS+ or the CS- (Fig.5). In these tufts, stimulus
547 preference after learning might be seeded by initially weak, directionally selective inputs on to
548 the neuron that already exist prior to conditioning and that are potentiated by the learning process.
549 We also found tufts that initially exhibited robust responses to both stimuli and either lost or
550 significantly reduced their response to one stimulus after learning. The reduction of an apical
551 response to a particular stimulus could be driven by local disynaptic inhibition between L5
552 pyramidal cells mediated by the apical-targeting Martinotti cells[85-87]. Through this mechanism, L5
553 neurons that are selective for a particular stimulus could inhibit responses to that stimulus in
554 neighboring L5 apical tufts. Experiments that assess the tuning of excitatory and inhibitory inputs
555 onto apical dendrites as a function of learning could test such mechanisms.

556

557 In addition to demonstrating increased tuft selectivity with learning, we replicated a surprising
558 phenomenon in a previous instrumental behavior in which a population of apical tufts exhibit
559 activity around the time of reward[28]. This reward-related activity was observed only during CS+
560 trials and was most prominent during intermediate conditioning sessions, when most animals
561 were still performing at chance levels, and disappeared completely by the final conditioning
562 session (Supp.Fig.1). Other than this transient effect, unconditioned stimuli did not appear to
563 elicit calcium responses, consistent with our previous findings[28]. The disappearance of this
564 reward-related peak might be attributable to the reward becoming predictable in later stages of
565 learning. In previous classical conditioning experiments, dopaminergic cells exhibit responses to
566 rewards early in learning due to the novelty of an unexpected stimulus. These responses are lost
567 after extended training, as animals learn the association between the CS and reward[88,89]. While
568 dopaminergic terminals are sparse in primary sensory areas, they are not entirely absent, nor are

dopaminergic receptors. Furthermore, the excitability of the apical tuft is sensitive to noradrenaline[26]. Interestingly, noradrenergic neurons in the locus coeruleus exhibit a similar phenomenon to dopaminergic neurons, where responses shift from temporal alignment with the reward to a predictive conditioned stimulus after learning[90]. Such mechanisms could explain why reward-related activity is restricted to early-to-intermediate learning in our paradigm.

Global versus local dendritic spikes

Apical dendrites exhibit not only global spikes that elicit calcium influx across the entire tuft, which we exclusively analyzed here, but also local events known as NMDA spikes, which typically engage short (<30-μm) segments of individual dendritic branches[15,31,57]. These local, NMDA receptor-dependent events can promote prolonged plasticity within individual dendritic branches in the absence of backpropagating actions potentials, a feature that is unique to the apical dendrites[16]. In motor cortex, branch-specific NMDA spikes are crucial for establishing the long-lasting plasticity necessary for learning[56], and depolarization provided by multiple local NMDA spikes is thought to be essential for the generation of a global calcium spike triggered by distal synaptic inputs[15]. We focused this study on global tuft-wide calcium events, rather than local events. Local events are more difficult to unambiguously identify in planar imaging[91], and their existence *in vivo* is still an open question for L5 apicals in barrel cortex[31,57]. Nonetheless, they may play important roles in plasticity processes that eventually lead to the emergence of global tuft spike selectivity for stimuli. Volumetric microscopy studies, the feasibility of which we showed here, are needed to further investigate the existence of local events in such behaviors as well as examine possible relationships between local and global tuft events during reinforcement learning. However, it would be essential to verify that seemingly spatially overlapping local and global events derive from the same dendritic tree, which requires greater resolution than was practical for the present study.

To analyze activity of individual tufts, we segmented these structures based on spatiotemporal covariance[45]. This method does not discount the possibility of errors where one tuft is split erroneously into two trees, or where two highly correlated tufts are merged. With this in mind, we used volumetric imaging SCAPE microscopy, which allowed us to visualize the apicals in three dimensions and unambiguously screen for such artifacts. The results from SCAPE are quantitatively similar to those from two-photon microscopy, and confirm that our observation of enhanced selectivity with learning is not an artifact of planar imaging.

Stability of learned tuft representations

In contrast to previous studies of discrimination learning[1-3], we included an unrewarded post-conditioning session to examine whether learning-related effects persisted through extinction. Our results show that post-conditioning selectivity of the apical population remains significantly higher than pre-conditioning, even after animals stop licking in response to the CS+ (Fig.8). Interestingly, the effects of learning are much more pronounced in animals that relied exclusively on their whiskers to perform the task. In animals that apparently used other sensory modalities, we observed a modest increase from the pre to last-rewarded session, which seemed to be largely absent by the post-conditioning session. Considering that these animals were additionally exploiting other sensory areas to perform, selectivity may have been more widely distributed and thus diluted in barrel cortex, diminishing the effect and its stability. How long selectivity persists in the neuronal population after conditioning and which factors influence stability are interesting open questions for future study.

Conclusion

In summary, we have shown for the first time that reinforcement learning enhances representations along behaviorally relevant dimensions in apical tufts. Our results suggest that dendritic calcium spikes are an important cellular mechanism underlying the changes in sensory

encoding that occur with learning, and provide an avenue for further investigation of cellular and circuit mechanisms underlying plasticity induced by perceptual experience and reinforcement. This cellular compartment may be key to understanding pathology in some cognitive, memory, and learning disorders.

ACKNOWLEDGEMENTS

We thank Venkatakaushik Voleti for help with the design, construction, and alignment of the SCAPE microscope; Dan Kato, Georgia Pierce, and Jung Park for help with pilot experiments; Eftychios Pnevmatikakis and Johannes Friedrich for advice on dendrite segmentation; and Larry Abbott, Stefano Fusi, Ashok Litwin-Kumar, Chris Rodgers, Georgia Pierce, Gordon Petty, and Dan Kato for comments on the manuscript. Funding was provided by a Wellcome Trust Discovery Award, an Academy of Medical Sciences Professorship, NIH/NINDS R01 NS069679, and NIH/NINDS R01 NS094659 (RMB); a Kavli Institute for Brain Science Postdoctoral Fellowship (SEB); NIH/NINDS/NIMH/BRAIN U01 NS094296, UF1 NS108213, U19 NS104649, and RF1 MH114276 (EMCH).

AUTHOR CONTRIBUTIONS

SEB and RMB conceived of the behavioral and two-photon imaging experiments. EMCH and RMB conceived of the SCAPE imaging experiments. SEB built the behavioral apparatus, EMCH, KBP, and CC designed, built, and maintained the SCAPE microscope, and RMB built and maintained the two-photon and intrinsic signal microscopes. SEB performed the experiments and analyzed the data with input from RMB and EMCH. SEB and RMB wrote the manuscript.

DATA AVAILABILITY

Due to the large volume of data (~80TB), data are maintained by the authors and available upon request.

647 **MAIN FIGURES**

648

649 **Fig. 1 | Mice rapidly learn to discriminate stimulus direction in head-fixed paradigm. a,** A
650 water droplet is paired with air puffs in one direction (CS+) but not the other (CS-). Licking in
651 anticipation of water is assessed in the response window just after CS+ or CS- and prior to water
652 delivery for the CS+ (grey bar). **b,** Experimental timeline. 2-3 weeks after virus injection, naive
653 tuft responses to stimuli are recorded (pre). The CS+ is then paired with water for 8-9 days (blue).
654 On the last day, stimuli are presented without reward (post). In a separate group of mice, the same
655 stimuli are presented over 9 days in the absence of reward (unrewarded group). **c,** Lick rasters for
656 three different sessions in one example mouse. On session 9, the CS+ but not the CS- reliably
657 elicits licks. **d,** Mean baseline-subtracted whisking amplitude aligned to the CS+ (red) and CS-
658 (navy) across sessions 1, 2, and 9 of an example mouse. **e,** Learning curve demonstrates rapid
659 learning. Mean probability of at least one lick in the response window across sessions. **f,**
660 Behavioral performance of each mouse in the rewarded group (M1 – M7).

661

662 **Fig. 2 | Overall tuft response to stimuli is unbiased and relatively stable across conditioning.**
663 **a,** Dendritic activity was recorded in layer 1 (i) in the C1/C2 barrel columns (ii). (i) Two-photon
664 image ~60 µm deep relative to pia. Dashed yellow lines denote C1 and C2 boundaries from
665 intrinsic imaging. Reconstruction from[50]. (ii) Tangential section through layer 4 showing barrels
666 stained with streptavidin-Alexa 647 and GCaMP6f-expressing apical trunks. Red circles indicate
667 location of 2-photon lesions to mark the imaging region for post-hoc analysis. **b,** Overlay of five
668 segmented pseudo-colored tufts from imaging field in A(i). **c,** Time courses of calcium responses
669 of example tufts in **b** to three air puffs (dashes). **d,** Amplitude for CS+ (red) and CS- responses
670 (blue), computed for each segmented tuft in the first 1.5 s post-stimulus (grey points), do not
671 differ within or across sessions. Colored lines indicate median. **e,** Same as in **d**, showing data for
672 all conditioning sessions.

Fig. 3 | Reinforcement learning, but not stimulus exposure, enhances tuft selectivity for CS+ and CS- stimuli. a, Across the indicated sessions, individual tufts (circles) exhibit larger biases to CS+ or CS- (pooled across all conditioned mice). **b,** Repeated exposure to stimuli does not bias individual tufts to CS+ or CS-. **c,** Conditioning reshapes distribution of selectivity indices for tufts from Normal on pre-conditioning session to uniform on post-conditioning session. **d,** Distribution of tuft selectivity indices remains Normal throughout all repeated exposure sessions. **e,** Selectivity (median SI magnitude of tufts for each session) increases with behavioral performance of 6 animals. **f,** Neural discriminability (mean ± sem) of tufts, pooled across all animals on each session, increases with conditioning and decreases with repeated exposure.

Fig. 4 | High-speed volumetric imaging of apical tufts confirms the emergence of enhanced selectivity after learning. a, Top and side view of four example tufts segmented from volumetric SCAPE imaging. **b,** Time courses of calcium activity from example tufts in **a** during five presentations of air puff stimuli (dashes). **c,** Performance across all conditioning sessions of two mice that were imaged with SCAPE. **d,** Across the indicated sessions, individual SCAPE-imaged tufts (circles) exhibit larger biases to CS+ or CS-. **e,** Conditioning reshapes selectivity distribution from Normal to uniform.

Fig. 5 | Longitudinal tracking reveals that reward enhances the selectivity of both initially unresponsive and responsive tufts. a, Three example tufts that were longitudinally tracked across learning. Top row: An initially unresponsive tuft develops a robust response to the CS+ but not the CS- after learning. Middle row: A responsive but unselective tuft loses its robust CS+ response and becomes selective for the CS-. Bottom row: A CS- selective neuron becomes unresponsive to both stimuli. **b,** Tufts that were unresponsive during the first session were longitudinally tracked to the last session. Plotted is the mean proportion of selective and

699 unselective neurons across all animals in the conditioned (black bars) and repeated exposure
700 (grey bars) groups. **c,d,** Same analysis as **b** for initially selective (**c**) and unselective (**d**) tufts.
701 Two-sample t-test was used for comparisons between conditioned and repeated exposure groups.
702 Paired t-test was used for comparisons within a group. * $p < 0.05$. **e,** Total tuft counts from first to
703 last session within the 3 response categories for either conditioned (left) or repeated exposure
704 (right) groups. **f,** SI of responsive tufts on the last session that were initially unresponsive during
705 the first session. Conditioned tufts have enhanced selectivity compared to repeated exposure. **g,**
706 Tufts that were selective on the last session are more selective if conditioned (black) rather than
707 undergoing repeated exposure (grey). **h,** Tufts that responded on both pre and post sessions tend
708 to have higher selectivity if conditioned rather than undergoing repeated exposure. **i,** SI of
709 responsive tufts on the first session that later became unresponsive during the last session.
710
711 **Fig. 6 | Whisking is only weakly correlated with tuft activity and cannot account for changes**
712 **in selectivity during learning. a,** Whisking amplitude aligned to calcium activity of three
713 example tufts in one session. Green shading indicates periods of whisking. Red and navy ticks
714 indicate CS+ or CS- delivery, respectively. **b,** Mean whisking response of five mice to CS+ (red)
715 and CS- (navy) does not change across sessions during learning (mean ± s.e.m.). **c,** Mean
716 standard deviation of whisking decreases for both CS+ and CS- across learning, but CS+ and CS-
717 do not differ. **d,** Event-triggered averages of 322 tufts on the post-conditioning day (grey traces -
718 individual tufts, black inset - population average) are responsive to stimuli but relatively
719 unmodulated by whisking. **e,** R^2 values for linear models predicting calcium from stimuli (y axis)
720 are consistently greater than those predicting calcium from whisking (x axis). Each circle
721 represents a tuft. (n = 322 tufts) **f,** Magnitude of tuft selectivity does not correlate with mean
722 whisking amplitude during CS+ (left) and CS- trials (right) on that session.
723

Fig. 7 | Behavioral responses do not account for enhancement of stimulus selectivity during learning. a, Mean stimulus responses of four tufts during hit (red), CR (cyan), and FA (black) trials. Top row: Example tufts whose responses are not behaviorally modulated (CR is similar to FA). Bottom row: Example tufts with behaviorally modulated responses (CR and FA differ). **b,** Selectivity index (SI) distribution changes from early (left) and late learning sessions (right) even when tufts with behaviorally modulated responses (CR≠FA) are excluded. **c,** Median SI magnitude of tufts in each of six animals (from panel **b**) increases from early to late learning sessions.

Fig. 8 | Apical tufts in barrel cortex of mice performing the task exclusively with their whiskers undergo long-lasting changes in selectivity. a, SI histograms of mice performing the task exclusively with their whiskers exhibit increased selectivity across pre-conditioning, last-rewarded, and post-conditioning sessions. **b,** Relative to pre-conditioning, mice using their whiskers and other sensory cues to perform the task have increased selectivity during the last rewarded session, but not the post-conditioning session. **c,** The probability of anticipatory licks in response to the CS+ extinguishes across post-conditioning blocks (of 20 trials each). **d,** Tuft selectively remains uniformly distributed during post-conditioning trial blocks 1-2 (top) while licking is extinguishing, and blocks 3-4 (bottom) in which licking is extinguished.

742 **METHODS**

743

744 All experiments complied with the NIH Guide for the Care and Use of Laboratory Animals and
745 were approved by the Institutional Animal Care and Use Committee of Columbia University.
746 Sixteen C57BL/6 mice ranging in age from 77 to 316 days old (mean of 123 days) were
747 used in these experiments. Six were male, and 10 female. Our results were observed in
748 both male and female individuals, and no sex difference was detected.

749

750 **Surgery**

751 Animals were administered dexamethasone (1 mg/kg) via intramuscular injection 1-4 hours prior
752 to surgery to reduce edema. Anesthesia was induced with 3% isoflurane in oxygen and
753 maintained at 1%. Mice were head-fixed in a stereotax, and a subcutaneous injection of
754 bupivacaine (0.5%, 0.1 mL) was administered under the scalp. Buprenorphine (0.05 mg/kg) was
755 injected subcutaneously on the back. The scalp was cut, and the skull was covered with a thin
756 layer of Vetbond. A circular craniotomy (3-mm diameter) centered at 1.5 mm posterior and 3.5
757 mm lateral to bregma was made using a dental drill. The dura was kept moist using artificial
758 cerebrospinal fluid.

759

760 For both two-photon and SCAPE microscopy, Rbp4-Cre_KL100 mice were injected with 100 nL
761 of virus (initial titer ~$2x10^{13}$ cfu/mL, diluted 1:4 in artificial cerebrospinal fluid) encoding
762 GCaMP6f in a Cre recombinase-specific manner (AAV1-CAG-flex-GCaMP6f, UPenn Vector
763 Core). The virus was injected in layer 5B of the barrel cortex (1.0 mm deep to the pia) using a
764 pulled pipette (20-30 μm ID) fastened on a Nanoject III, which was mounted on a manipulator
765 angled at ~30° from vertical. The depth was chosen to maximize labeling of thick-tufted
766 pyramidal neurons. In pilot experiments, we found that placing injections 1.0 mm deep resulted

767 primarily in thick-tufted labeling whereas at more superficial depths (e.g., 0.8 mm deep) we
768 obtained mainly thin-tufted tufts, consistent with ref [92]. The dura was then removed, and a thin
769 cover glass was implanted and sealed using superglue. A custom metal head plate was implanted
770 on the skull using dental cement. Twenty-four hours after surgery, carprofen (5 mg/kg) was
771 administered subcutaneously. Imaging and behavioral training commenced 3 weeks after surgery.
772
773 **Behavior**
774 Animals in both rewarded 'conditioning' and unrewarded 'repeated exposure' groups were water
775 restricted for 2 days prior to starting imaging and habituated to head fixation for ~10 minutes on
776 each of these 2 days. They were subsequently given ~1 mL of water per day for 9 days either by
777 pairing water rewards with a specific stimulus (conditioning group), or in their cage following the
778 imaging session (repeated exposure group). Mice were head restrained in a custom-made
779 behavioral apparatus by positioning the body in a 3D-printed chamber and fastening the head
780 plate to metal posts flanking the chamber. Air puff stimuli (10 psi measured before a control
781 solenoid, 100 ms) were delivered from two nozzles (cut P200 pipette tips) positioned toward the
782 distal tips of the whiskers, in either the rostrocaudal or ventrodorsal direction. Nozzles were
783 oriented to prevent air jets from stimulating other parts of the face. One of these directions (CS+)
784 was paired with a water reward (10 μL), delivered through a lick port 0.5 seconds after the
785 stimulus onset. The particular direction (rostrocaudal vs ventrodorsal) used as the CS+ was
786 randomized and counterbalanced across mice. Approximately 180 stimuli were presented over the
787 course of a 30-minute imaging session (8-12-s intertrial interval). The probability of CS+ or CS-
788 delivery was 50%. In preliminary experiments, we found that an auditory mask helped prevent
789 mice from exploiting auditory cues to discriminate the two stimuli: a third air nozzle was
790 positioned close to the mouse and was active throughout the session.
791

792 During the first session (pre-conditioning), stimuli were delivered in the absence of reward to
793 assess neural and behavioral responses in naïve animals. In the following 7-9 days, the CS+ was
794 paired with reward. Licks for rewards were detected with a capacitance-based touch sensor
795 (Sparkfun). A trial response was registered when one or more licks were elicited within a 0.5-
796 second response window following the stimulus and before reward delivery. To determine
797 whether behavioral performance was above chance, we computed 95% confidence intervals using
798 the 'binofit' function in MATLAB. During the final session (post-conditioning), stimuli were
799 delivered in the absence of reward. Animals in the unrewarded group received the same two
800 stimuli across 9 days without reward pairing. Behavioral experiments were performed with the
801 Arduino-based OpenMaze open-source behavioral system, whose designs are fully described at
802 www.openmaze.org. Whisking was monitored at 125 fps with a camera (Sony PS3eye) and
803 automatically tracked using published software [93].
804
805 **Intrinsic signal optical imaging and two-photon imaging**
806 Intrinsic signal optical imaging and two-photon imaging were performed on a Sutter movable
807 objective microscope. The locations of whisker barrels in S1 were identified using intrinsic signal
808 optical imaging. Single whiskers in isoflurane-anesthetized mice were stimulated at 5 Hz using a
809 piezoelectric bimorph while recording the reflectance of 700-nm long-pass incandescent light
810 with a Rolera CCD camera (QImaging) through a low-magnification objective (Zeiss
811 5X/0.16NA). Movies were collected using software custom-written in Labview (National
812 Instruments). Regions of reflectance change were referenced to an image acquired under green
813 illumination.
814
815 Two-photon imaging was conducted on the same microscope under the control of the ScanImage
816 software package (V. Iyer, Janelia Farms). All calcium imaging data was collected by two-photon
817 microscopy except for those in figure 4. Scanning during awake conditions was performed at 30

818 fps using a Chameleon Ultra II laser (Coherent) tuned to 920 nm, precompensated for group
819 velocity dispersion and focused through a 20x/1.0NA water immersion lens (Zeiss). Emitted light
820 was collected with an HQ535/50 filter (Chroma) and GaAsP photomultiplier tubes (Hamamatsu
821 Photonics). Apical tuft tufts in Layer 1 were imaged at depths of 40-80 μm from the pial surface
822 (433 x 433 μm field of view, 512 x 512 pixels).
823
824 **SCAPE imaging**
825 High-speed volumetric imaging was performed using a custom SCAPE microscope as previously
826 described, including for dendritic tufts[36,37,94]. Briefly, the cortex was illuminated with an oblique
827 light sheet through a Olympus XLUMPLFLN 20XW 1.0 NA water immersion objective with a 2-
828 mm working distance. Fluorescence excited by this sheet (extending in the *y*-*z′* direction) was
829 collected by the same objective lens. A galvanometer mirror in the system was positioned to both
830 cause the oblique light sheet to scan from side to side across the sample (in the *x* direction) but
831 also to de-scan returning fluorescence light. This optical path results in an intermediate, de-
832 scanned oblique image plane that is stationary yet always co-aligned with the plane in the sample
833 that is being illuminated by the scanning light sheet. Image rotation optics and a fast sCMOS
834 camera (Andor Zyla 4.2+) were then focused to capture these *y*-*z′* images (750 x 200 pixels) at
835 >1000 frames per second as the sheet was repeatedly scanned across the cortex in the *x* direction.
836 All other system parts, including the objective and sample stage, were stationary during high-
837 speed 3D image acquisition. Data were reformed into a 3D volume by stacking successive *y*-*z′*
838 planes according to the scanning mirror's *x* position and de-skewing to correct for the oblique
839 sheet angle. This rotation of the image volume is responsible for its rectangular
840 appearance despite the camera's square frames. The resulting volumes were large enough
841 to encompass many GCaMP6f-labeled tufts in barrel cortex,
842

843 In this study, the stationary objective lens in SCAPE was configured on a manual rotation mount
844 and set to 20º-30º away from the standard upright configuration, so the optical axis was
845 perpendicular to the cranial window to achieve optimal performance without tilting the head of
846 the animal. A 488-nm laser (Coherent OBIS) was used for excitation (<10 mW at the sample)
847 with a 500-nm long-pass filter in the emission path. To achieve optimal spatiotemporal resolution
848 and volume rate, the sample was imaged with an *x*-direction scanning step of 3 μm over a 300 ×
849 1050 × 234 μm field of view (*x*-*y*-*z*, 3.0 × 1.40 × 1.17 μm per voxel, 100 x 750 x 200 voxels) at
850 10 volumes per second (VPS). Our imaging involves no special practical considerations or
851 limitations of field of view or resolution, beyond the usual imaging goal of maximizing
852 FOV while maintaining sufficient resolution to discern structures of interest (dendrites).
853
854 **Analysis**
855 Two-photon movies were motion corrected using the NormCorre package [95] in MATLAB. Spatial
856 and temporal components for individual tufts imaged by two-photon and SCAPE were segmented
857 using CaImAn v1.8.3, which employs large-scale sparse non-negative matrix factorization [45,96].
858 CaImAn inherently corrects for background signal. All further analyses used custom-written
859 routines implemented in MATLAB. Spatial components with tuft structural characteristics were
860 identified and analyzed, while neuropil components were discarded.
861
862 To quantify a tuft's response to stimuli, the mean stimulus-aligned ΔF/F was computed across all
863 CS+ or CS- trials and corrected by the mean ΔF/F of the second before the trial. Probability of
864 transients was obtained by taking each trial's ΔF/F in the first 1.5 seconds following either the
865 CS+ or CS- and fitting these data with a univariate mixture of two Normal distributions: $(1-$
866 $p)N(\mu_1, \sigma_1) + pN(\mu_2, \sigma_2)$. The smaller Normal reflects the distribution of failures, and the larger

867 Normal the distribution of transient amplitudes following the stimulus. The parameter *p* captures
868 the probability of transients.
869
870 From these data, a selectivity index (SI) was defined as $(F_{CS+} - F_{CS-}) / (F_{CS+} + F_{CS-})$, in which F_{CS+}
871 and F_{CS-} are the mean stimulus-aligned amplitudes (ΔF/F) to the CS+ and CS- within the first 1.5
872 seconds, respectively. This yielded values that range from -1 (exclusively CS- responsive) to 1
873 (exclusively CS+ responsive). Neural discriminability was defined as $d' = |F_{CS+} - F_{CS-}| / \sqrt{((\sigma^2_{CS+}}$
874 $+ \sigma^2_{CS-})/2)$ where σ^2_{CS+} is the variance of the response amplitudes in F_{CS+} and σ^2_{CS-} is the variance
875 of the response amplitudes in F_{CS-}.
876
877 For longitudinal analysis, tufts were categorized as stimulus responsive if they met two criteria:
878 1) Across all trials, the mean ΔF/F 1.5 seconds before and 1.5 seconds after the stimulus were
879 significantly different according to the Wilcoxon rank sum test, for either the CS+ or CS-, and 2)
880 the average response amplitude for that stimulus was greater than 0.04 ΔF/F. Tufts with a
881 significant response to only one stimulus were categorized as highly selective and their |SI| was
882 set to 1. To classify tufts as behaviorally modulated, the mean ΔF/F of the first 1.5 seconds after
883 the stimulus was computed for false alarm and correct rejection trials and compared with a rank
884 sum test. Only sessions with at least 12 false alarm trials were used for this analysis. If the two
885 distributions were significantly different, the tuft was classified as behaviorally modulated.
886
887 Custom MATLAB software was used to compute the median whisker angle, and whisking
888 amplitude was computed as described previously [97]. The median angle was bandpass filtered from
889 4 to 30 Hz and passed through a Hilbert transform to calculate phase. We defined the upper and
890 lower envelopes of the unfiltered median whisking angle as the points in the whisk cycle where
891 phase equaled 0 (most protracted) or π (most retracted), respectively. Whisking amplitude was

defined as the difference between these two envelopes. Periods of whisking were defined as times where whisking amplitude exceeded 20% of maximum for at least 250 msec. Periods of time where amplitude exceeded this threshold for less than 250 msec were considered ambiguous and excluded from analysis of whisking versus quiescence. The whisking-triggered average for each tuft was computed by aligning the calcium signal to the start times of whisking periods during inter-trial intervals (2-8 seconds after stimulus delivery).

For the linear regression analysis, we excerpted the calcium timeseries 2 seconds before and 6 seconds after each stimulus onset. The whisking amplitude signal was frame aligned to the calcium signal according to the lag of the calcium-whisking cross-correlation peak for each tuft. Whisking amplitude was then normalized to the max, yielding values that ranged from 0 to 1. The stimulus predictor variable was a binary vector with an 800-msec 'on' period (24 frames) centered at the stimulus time. The timing of the stimulus variable was then aligned to the calcium signal according to the latency of peak of the mean $\Delta F/F$ of the first 1.5 seconds relative to the stimulus. The lick predictor variable was a binary vector with 'on' periods denoting lick bouts. Lick bouts were defined as periods of time where the mouse elicited at least 2 licks, with a maximum gap of 200 msec, and therefore had variable lengths.

All statistical tests were two-sided. T-tests were used for Normally distributed data. Otherwise non-parametric tests were applied.

References

1 Poort, J. *et al.* Learning Enhances Sensory and Multiple Non-sensory Representations in Primary Visual Cortex. *Neuron* **86**, 1478-1490, doi:10.1016/j.neuron.2015.05.037 (2015).

2 Liu, D. *et al.* Orbitofrontal control of visual cortex gain promotes visual associative learning. *Nat Commun* **11**, 2784, doi:10.1038/s41467-020-16609-7 (2020).

3 Henschke, J. U. *et al.* Reward Association Enhances Stimulus-Specific Representations in Primary Visual Cortex. *Curr Biol* **30**, 1866-1880 e1865, doi:10.1016/j.cub.2020.03.018 (2020).

4 Beitel, R. E., Schreiner, C. E., Cheung, S. W., Wang, X. & Merzenich, M. M. Reward-dependent plasticity in the primary auditory cortex of adult monkeys trained to discriminate temporally modulated signals. *Proc Natl Acad Sci U S A* **100**, 11070-11075, doi:10.1073/pnas.1334187100 (2003).

5 Goltstein, P. M., Coffey, E. B., Roelfsema, P. R. & Pennartz, C. M. In vivo two-photon Ca2+ imaging reveals selective reward effects on stimulus-specific assemblies in mouse visual cortex. *J Neurosci* **33**, 11540-11555, doi:10.1523/JNEUROSCI.1341-12.2013 (2013).

6 David, S. V., Fritz, J. B. & Shamma, S. A. Task reward structure shapes rapid receptive field plasticity in auditory cortex. *Proc Natl Acad Sci U S A* **109**, 2144-2149, doi:10.1073/pnas.1117717109 (2012).

7 Fritz, J., Shamma, S., Elhilali, M. & Klein, D. Rapid task-related plasticity of spectrotemporal receptive fields in primary auditory cortex. *Nat Neurosci* **6**, 1216-1223, doi:10.1038/nn1141 (2003).

8 Banerjee, A. *et al.* Value-guided remapping of sensory cortex by lateral orbitofrontal cortex. *Nature* **585**, 245-250, doi:10.1038/s41586-020-2704-z (2020).

9 Zhang, W. & Bruno, R. M. High-order thalamic inputs to primary somatosensory cortex are stronger and longer lasting than cortical inputs. *eLife* **8**, doi:10.7554/eLife.44158 (2019).

10 Rubio-Garrido, P., Perez-de-Manzo, F., Porrero, C., Galazo, M. J. & Clasca, F. Thalamic input to distal apical dendrites in neocortical layer 1 is massive and highly convergent. *Cereb Cortex* **19**, 2380-2395, doi:10.1093/cercor/bhn259 (2009).

11 Cauller, L. J., Clancy, B. & Connors, B. W. Backward cortical projections to primary somatosensory cortex in rats extend long horizontal axons in layer I. *J Comp Neurol* **390**, 297-310 (1998).

12 Amitai, Y., Friedman, A., Connors, B. W. & Gutnick, M. J. Regenerative activity in apical dendrites of pyramidal cells in neocortex. *Cereb Cortex* **3**, 26-38 (1993).

13 Yuste, R., Gutnick, M. J., Saar, D., Delaney, K. R. & Tank, D. W. Ca2+ accumulations in dendrites of neocortical pyramidal neurons: an apical band and evidence for two functional compartments. *Neuron* **13**, 23-43 (1994).

14 Schiller, J., Schiller, Y., Stuart, G. & Sakmann, B. Calcium action potentials restricted to distal apical dendrites of rat neocortical pyramidal neurons. *J Physiol* **505 (Pt 3)**, 605-616 (1997).

15 Larkum, M. E., Nevian, T., Sandler, M., Polsky, A. & Schiller, J. Synaptic integration in tuft dendrites of layer 5 pyramidal neurons: a new unifying principle. *Science* **325**, 756-760, doi:10.1126/science.1171958 (2009).

16 Sandler, M., Shulman, Y. & Schiller, J. A Novel Form of Local Plasticity in Tuft Dendrites of Neocortical Somatosensory Layer 5 Pyramidal Neurons. *Neuron* **90**, 1028-1042, doi:10.1016/j.neuron.2016.04.032 (2016).

17 Manita, S. *et al.* A Top-Down Cortical Circuit for Accurate Sensory Perception. *Neuron* **86**, 1304-1316, doi:10.1016/j.neuron.2015.05.006 (2015).

18 Roelfsema, P. R. & Holtmaat, A. Control of synaptic plasticity in deep cortical networks. *Nat Rev Neurosci* **19**, 166-180, doi:10.1038/nrn.2018.6 (2018).

19 Larkum, M. E. & Zhu, J. J. Signaling of layer 1 and whisker-evoked Ca2+ and Na+ action potentials in distal and terminal dendrites of rat neocortical pyramidal neurons in vitro and in vivo. *J Neurosci* **22**, 6991-7005, doi:20026717 (2002).

20 Larkum, M. E., Senn, W. & Luscher, H. R. Top-down dendritic input increases the gain of layer 5 pyramidal neurons. *Cereb Cortex* **14**, 1059-1070, doi:10.1093/cercor/bhh065 (2004).

21 Schwindt, P. & Crill, W. Mechanisms underlying burst and regular spiking evoked by dendritic depolarization in layer 5 cortical pyramidal neurons. *J Neurophysiol* **81**, 1341-1354, doi:10.1152/jn.1999.81.3.1341 (1999).

22 Larkum, M. E., Zhu, J. J. & Sakmann, B. Dendritic mechanisms underlying the coupling of the dendritic with the axonal action potential initiation zone of adult rat layer 5 pyramidal neurons. *J Physiol* **533**, 447-466 (2001).

23 Manita, S., Miyakawa, H., Kitamura, K. & Murayama, M. Dendritic Spikes in Sensory Perception. *Front Cell Neurosci* **11**, 29, doi:10.3389/fncel.2017.00029 (2017).

24 Francioni, V., Padamsey, Z. & Rochefort, N. L. High and asymmetric somato-dendritic coupling of V1 layer 5 neurons independent of visual stimulation and locomotion. *Elife* **8**, doi:10.7554/eLife.49145 (2019).

25 Beaulieu-Laroche, L., Toloza, E. H. S., Brown, N. J. & Harnett, M. T. Widespread and Highly Correlated Somato-dendritic Activity in Cortical Layer 5 Neurons. *Neuron* **103**, 235-241 e234, doi:10.1016/j.neuron.2019.05.014 (2019).

26 Labarrera, C. *et al.* Adrenergic Modulation Regulates the Dendritic Excitability of Layer 5 Pyramidal Neurons In Vivo. *Cell Rep* **23**, 1034-1044, doi:10.1016/j.celrep.2018.03.103 (2018).

27 Brombas, A., Fletcher, L. N. & Williams, S. R. Activity-dependent modulation of layer 1 inhibitory neocortical circuits by acetylcholine. *J Neurosci* **34**, 1932-1941, doi:10.1523/JNEUROSCI.4470-13.2014 (2014).

28 Lacefield, C. O., Pnevmatikakis, E. A., Paninski, L. & Bruno, R. M. Reinforcement Learning Recruits Somata and Apical Dendrites across Layers of Primary Sensory Cortex. *Cell Rep* **26**, 2000-2008 e2002, doi:10.1016/j.celrep.2019.01.093 (2019).

29 Luebke, J. I. *et al.* Dendritic vulnerability in neurodegenerative disease: insights from analyses of cortical pyramidal neurons in transgenic mouse models. *Brain Struct Funct* **214**, 181-199, doi:10.1007/s00429-010-0244-2 (2010).

30 Tsai, J., Grutzendler, J., Duff, K. & Gan, W. B. Fibrillar amyloid deposition leads to local synaptic abnormalities and breakage of neuronal branches. *Nat Neurosci* **7**, 1181-1183, doi:10.1038/nn1335 (2004).

31 Xu, N. L. *et al.* Nonlinear dendritic integration of sensory and motor input during an active sensing task. *Nature* **492**, 247-251, doi:10.1038/nature11601 (2012).

32 Takahashi, N. *et al.* Active dendritic currents gate descending cortical outputs in perception. *Nat Neurosci*, doi:10.1038/s41593-020-0677-8 (2020).

33 Takahashi, N., Oertner, T. G., Hegemann, P. & Larkum, M. E. Active cortical dendrites modulate perception. *Science* **354**, 1587-1590, doi:10.1126/science.aah6066 (2016).

34 Bittner, K. C., Milstein, A. D., Grienberger, C., Romani, S. & Magee, J. C. Behavioral time scale synaptic plasticity underlies CA1 place fields. *Science* **357**, 1033-1036, doi:10.1126/science.aan3846 (2017).

35 Doron, G. *et al.* Perirhinal input to neocortical layer 1 controls learning. *Science* **370**, doi:10.1126/science.aaz3136 (2020).

36 Bouchard, M. B. *et al.* Swept confocally-aligned planar excitation (SCAPE) microscopy for high speed volumetric imaging of behaving organisms. *Nat Photonics* **9**, 113-119, doi:10.1038/nphoton.2014.323 (2015).

37 Hillman, E. M. *et al.* High-speed 3D imaging of cellular activity in the brain using axially-extended beams and light sheets. *Curr Opin Neurobiol* **50**, 190-200 (2018).
38 Yu, Y. S., Graff, M. M., Bresee, C. S., Man, Y. B. & Hartmann, M. J. Whiskers aid anemotaxis in rats. *Sci Adv* **2**, e1600716, doi:10.1126/sciadv.1600716 (2016).
39 Yu, Y. S., Graff, M. M. & Hartmann, M. J. Mechanical responses of rat vibrissae to airflow. *J Exp Biol* **219**, 937-948, doi:10.1242/jeb.126896 (2016).
40 Nakamura, S., Narumi, T., Tsutsui, K. & Iijima, T. Difference in the functional significance between the lemniscal and paralemniscal pathways in the perception of direction of single-whisker stimulation examined by muscimol microinjection. *Neurosci Res* **64**, 323-329, doi:10.1016/j.neures.2009.04.005 (2009).
41 Bernhard, S. M. *et al.* An automated homecage system for multiwhisker detection and discrimination learning in mice. *PLoS One* **15**, e0232916, doi:10.1371/journal.pone.0232916 (2020).
42 Chen, T. W. *et al.* Ultrasensitive fluorescent proteins for imaging neuronal activity. *Nature* **499**, 295-300, doi:10.1038/nature12354 (2013).
43 Kozorovitskiy, Y., Saunders, A., Johnson, C. A., Lowell, B. B. & Sabatini, B. L. Recurrent network activity drives striatal synaptogenesis. *Nature* **485**, 646-650, doi:10.1038/nature11052 (2012).
44 Glickfeld, L. L., Andermann, M. L., Bonin, V. & Reid, R. C. Cortico-cortical projections in mouse visual cortex are functionally target specific. *Nat Neurosci* **16**, 219-226, doi:10.1038/nn.3300 (2013).
45 Giovannucci, A. *et al.* CaImAn an open source tool for scalable calcium imaging data analysis. *Elife* **8**, doi:10.7554/eLife.38173 (2019).
46 Pakan, J. M. P., Currie, S. P., Fischer, L. & Rochefort, N. L. The Impact of Visual Cues, Reward, and Motor Feedback on the Representation of Behaviorally Relevant Spatial Locations in Primary Visual Cortex. *Cell Rep* **24**, 2521-2528, doi:10.1016/j.celrep.2018.08.010 (2018).
47 Wang, P. Y. *et al.* Transient and Persistent Representations of Odor Value in Prefrontal Cortex. *Neuron* **108**, 209-224 e206, doi:10.1016/j.neuron.2020.07.033 (2020).
48 Bruno, R. M., Khatri, V., Land, P. W. & Simons, D. J. Thalamocortical angular tuning domains within individual barrels of rat somatosensory cortex. *J Neurosci* **23**, 9565-9574 (2003).
49 Bruno, R. M. & Sakmann, B. Cortex is driven by weak but synchronously active thalamocortical synapses. *Science* **312**, 1622-1627, doi:10.1126/science.1124593 (2006).
50 Ramirez, A. *et al.* Spatiotemporal receptive fields of barrel cortex revealed by reverse correlation of synaptic input. *Nat Neurosci* **17**, 866-875, doi:10.1038/nn.3720 (2014).
51 Yao, H. & Dan, Y. Stimulus timing-dependent plasticity in cortical processing of orientation. *Neuron* **32**, 315-323, doi:10.1016/s0896-6273(01)00460-3 (2001).
52 Dragoi, V., Sharma, J., Miller, E. K. & Sur, M. Dynamics of neuronal sensitivity in visual cortex and local feature discrimination. *Nat Neurosci* **5**, 883-891, doi:10.1038/nn900 (2002).
53 Dragoi, V., Sharma, J. & Sur, M. Adaptation-induced plasticity of orientation tuning in adult visual cortex. *Neuron* **28**, 287-298, doi:10.1016/s0896-6273(00)00103-3 (2000).
54 Zhang, Y., Cudmore, R. H., Lin, D. T., Linden, D. J. & Huganir, R. L. Visualization of NMDA receptor-dependent AMPA receptor synaptic plasticity in vivo. *Nat Neurosci* **18**, 402-407, doi:10.1038/nn.3936 (2015).
55 Chu, M. W., Li, W. L. & Komiyama, T. Balancing the Robustness and Efficiency of Odor Representations during Learning. *Neuron* **92**, 174-186, doi:10.1016/j.neuron.2016.09.004 (2016).
56 Cichon, J. & Gan, W. B. Branch-specific dendritic Ca(2+) spikes cause persistent synaptic plasticity. *Nature* **520**, 180-185, doi:10.1038/nature14251 (2015).

57 Palmer, L. M. *et al.* NMDA spikes enhance action potential generation during sensory input. *Nat Neurosci* **17**, 383-390, doi:10.1038/nn.3646 (2014).
58 Derdikman, D. *et al.* Layer-specific touch-dependent facilitation and depression in the somatosensory cortex during active whisking. *J Neurosci* **26**, 9538-9547, doi:10.1523/JNEUROSCI.0918-06.2006 (2006).
59 de Kock, C. P. & Sakmann, B. Spiking in primary somatosensory cortex during natural whisking in awake head-restrained rats is cell-type specific. *Proc Natl Acad Sci U S A* **106**, 16446-16450, doi:10.1073/pnas.0904143106 (2009).
60 Rodgers, C. C. *et al.* Sensorimotor strategies and neuronal representations for shape discrimination. *Neuron* **109**, 2308-2325 e2310, doi:10.1016/j.neuron.2021.05.019 (2021).
61 Larkum, M. A cellular mechanism for cortical associations: an organizing principle for the cerebral cortex. *Trends Neurosci* **36**, 141-151, doi:10.1016/j.tins.2012.11.006 (2013).
62 Park, J. M. *et al.* Deep and superficial layers of the primary somatosensory cortex are critical for whisker-based texture discrimination in mice. *bioRxiv*, 2020.2008.2012.245381, doi:10.1101/2020.08.12.245381 (2020).
63 Rigotti, M. *et al.* The importance of mixed selectivity in complex cognitive tasks. *Nature* **497**, 585-590, doi:10.1038/nature12160 (2013).
64 Stringer, C., Pachitariu, M., Steinmetz, N., Carandini, M. & Harris, K. D. High-dimensional geometry of population responses in visual cortex. *Nature* **571**, 361-365, doi:10.1038/s41586-019-1346-5 (2019).
65 Kim, J., Erskine, A., Cheung, J. A. & Hires, S. A. Behavioral and Neural Bases of Tactile Shape Discrimination Learning in Head-Fixed Mice. *Neuron* **108**, 953-967 e958, doi:10.1016/j.neuron.2020.09.012 (2020).
66 Dabney, W. *et al.* A distributional code for value in dopamine-based reinforcement learning. *Nature* **577**, 671-675, doi:10.1038/s41586-019-1924-6 (2020).
67 Petreanu, L. *et al.* Activity in motor-sensory projections reveals distributed coding in somatosensation. *Nature* **489**, 299-303, doi:10.1038/nature11321 (2012).
68 Wimmer, V. C., Bruno, R. M., de Kock, C. P., Kuner, T. & Sakmann, B. Dimensions of a Projection Column and Architecture of VPM and POm Axons in Rat Vibrissal Cortex. *Cereb Cortex* **20**, 2265-2276, doi:bhq068 [pii] 10.1093/cercor/bhq068 (2010).
69 Feldmeyer, D. Excitatory neuronal connectivity in the barrel cortex. *Front Neuroanat* **6**, 24, doi:10.3389/fnana.2012.00024 (2012).
70 Constantinople, C. M. & Bruno, R. M. Deep cortical layers are activated directly by thalamus. *Science* **340**, 1591-1594, doi:10.1126/science.1236425 (2013).
71 Petersen, C. C. & Crochet, S. Synaptic computation and sensory processing in neocortical layer 2/3. *Neuron* **78**, 28-48, doi:10.1016/j.neuron.2013.03.020 (2013).
72 Yamashita, T. *et al.* Diverse Long-Range Axonal Projections of Excitatory Layer 2/3 Neurons in Mouse Barrel Cortex. *Front Neuroanat* **12**, 33, doi:10.3389/fnana.2018.00033 (2018).
73 Llinas, R., Ribary, U., Contreras, D. & Pedroarena, C. The neuronal basis for consciousness. *Philos Trans R Soc Lond B Biol Sci* **353**, 1841-1849, doi:10.1098/rstb.1998.0336 (1998).
74 Krauzlis, R. J., Lovejoy, L. P. & Zenon, A. Superior colliculus and visual spatial attention. *Annu Rev Neurosci* **36**, 165-182, doi:10.1146/annurev-neuro-062012-170249 (2013).
75 Parvizi, J. & Damasio, A. Consciousness and the brainstem. *Cognition* **79**, 135-160, doi:10.1016/s0010-0277(00)00127-x (2001).
76 Feldman, D. E. & Brecht, M. Map plasticity in somatosensory cortex. *Science* **310**, 810-815, doi:10.1126/science.1115807 (2005).

77 Mechawar, N., Cozzari, C. & Descarries, L. Cholinergic innervation in adult rat cerebral cortex: a quantitative immunocytochemical description. *J Comp Neurol* **428**, 305-318 (2000).

78 Freedman, R., Foote, S. L. & Bloom, F. E. Histochemical characterization of a neocortical projection of the nucleus locus coeruleus in the squirrel monkey. *J Comp Neurol* **164**, 209-231, doi:10.1002/cne.901640205 (1975).

79 Chubykin, A. A., Roach, E. B., Bear, M. F. & Shuler, M. G. A cholinergic mechanism for reward timing within primary visual cortex. *Neuron* **77**, 723-735, doi:10.1016/j.neuron.2012.12.039 (2013).

80 Thiele, A. & Bellgrove, M. A. Neuromodulation of Attention. *Neuron* **97**, 769-785, doi:10.1016/j.neuron.2018.01.008 (2018).

81 Hangya, B., Ranade, S. P., Lorenc, M. & Kepecs, A. Central Cholinergic Neurons Are Rapidly Recruited by Reinforcement Feedback. *Cell* **162**, 1155-1168, doi:10.1016/j.cell.2015.07.057 (2015).

82 Froemke, R. C., Merzenich, M. M. & Schreiner, C. E. A synaptic memory trace for cortical receptive field plasticity. *Nature* **450**, 425-429, doi:10.1038/nature06289 (2007).

83 Letzkus, J. J. *et al.* A disinhibitory microcircuit for associative fear learning in the auditory cortex. *Nature* **480**, 331-335, doi:10.1038/nature10674 (2011).

84 Gasselin, C., Hohl, B., Vernet, A., Crochet, S. & Petersen, C. C. H. Cell-type-specific nicotinic input disinhibits mouse barrel cortex during active sensing. *Neuron*, doi:10.1016/j.neuron.2020.12.018 (2021).

85 Berger, T. K., Silberberg, G., Perin, R. & Markram, H. Brief bursts self-inhibit and correlate the pyramidal network. *PLoS Biol* **8**, doi:10.1371/journal.pbio.1000473 (2010).

86 Kapfer, C., Glickfeld, L. L., Atallah, B. V. & Scanziani, M. Supralinear increase of recurrent inhibition during sparse activity in the somatosensory cortex. *Nat Neurosci* **10**, 743-753, doi:10.1038/nn1909 (2007).

87 Naka, A. & Adesnik, H. Inhibitory Circuits in Cortical Layer 5. *Front Neural Circuits* **10**, 35, doi:10.3389/fncir.2016.00035 (2016).

88 Ljungberg, T., Apicella, P. & Schultz, W. Responses of monkey dopamine neurons during learning of behavioral reactions. *J Neurophysiol* **67**, 145-163, doi:10.1152/jn.1992.67.1.145 (1992).

89 Pan, W. X., Schmidt, R., Wickens, J. R. & Hyland, B. I. Dopamine cells respond to predicted events during classical conditioning: evidence for eligibility traces in the reward-learning network. *J Neurosci* **25**, 6235-6242, doi:10.1523/JNEUROSCI.1478-05.2005 (2005).

90 Bouret, S. & Sara, S. J. Reward expectation, orientation of attention and locus coeruleus-medial frontal cortex interplay during learning. *Eur J Neurosci* **20**, 791-802, doi:10.1111/j.1460-9568.2004.03526.x (2004).

91 Sheffield, M. E. & Dombeck, D. A. Calcium transient prevalence across the dendritic arbour predicts place field properties. *Nature* **517**, 200-204, doi:10.1038/nature13871 (2015).

92 Oberlaender, M. *et al.* Cell type-specific three-dimensional structure of thalamocortical circuits in a column of rat vibrissal cortex. *Cereb Cortex* **22**, 2375-2391, doi:10.1093/cercor/bhr317 (2012).

93 Clack, N. G. *et al.* Automated tracking of whiskers in videos of head fixed rodents. *PLoS Comput Biol* **8**, e1002591, doi:10.1371/journal.pcbi.1002591 (2012).

94 Voleti, V. *et al.* Real-time volumetric microscopy of in vivo dynamics and large-scale samples with SCAPE 2.0. *Nat Methods* **16**, 1054-1062, doi:10.1038/s41592-019-0579-4 (2019).

95 Pnevmatikakis, E. A. & Giovannucci, A. NoRMCorre: An online algorithm for piecewise rigid motion correction of calcium imaging data. *J Neurosci Methods* **291**, 83-94, doi:10.1016/j.jneumeth.2017.07.031 (2017).

96 Pnevmatikakis, E. A. *et al.* Simultaneous Denoising, Deconvolution, and Demixing of Calcium Imaging Data. *Neuron* **89**, 285-299, doi:10.1016/j.neuron.2015.11.037 (2016).

97 Petty, G. H., Kinnischtzke, A. K., Hong, Y. K. & Bruno, R. M. Effects of arousal and movement on secondary somatosensory and visual thalamus. *bioRxiv*, 2020.2003.2004.977348, doi:10.1101/2020.03.04.977348 (2020).

Figure 1

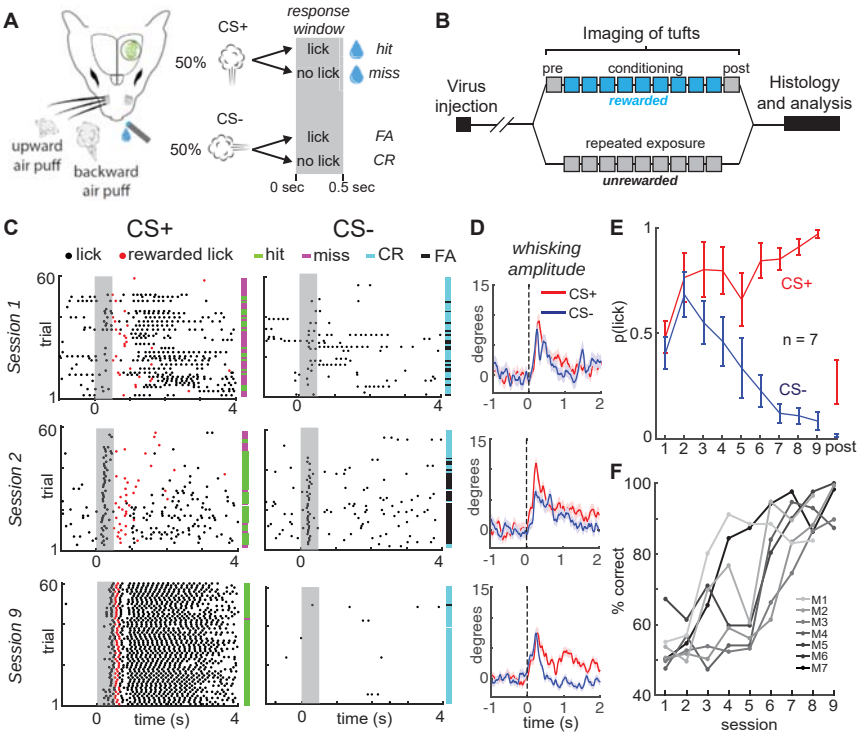
A
upward air puff
backward air puff
CS+
50%
response window
lick
no lick
hit
miss
CS-
50%
lick
no lick
FA
CR
0 sec
0.5 sec
B
Imaging of tufts
Virus injection
pre
conditioning
post
rewarded
repeated exposure
unrewarded
Histology and analysis
C
CS+
CS-
lick
rewarded lick
hit
miss
CR
FA
Session 1
Session 2
Session 9
trial
time (s)
D
whisking amplitude
CS+
CS-
degrees
time (s)
E
p(lick)
CS+
CS-
n = 7
post
F
% correct
session
M1
M2
M3
M4
M5
M6
M7

Figure 2

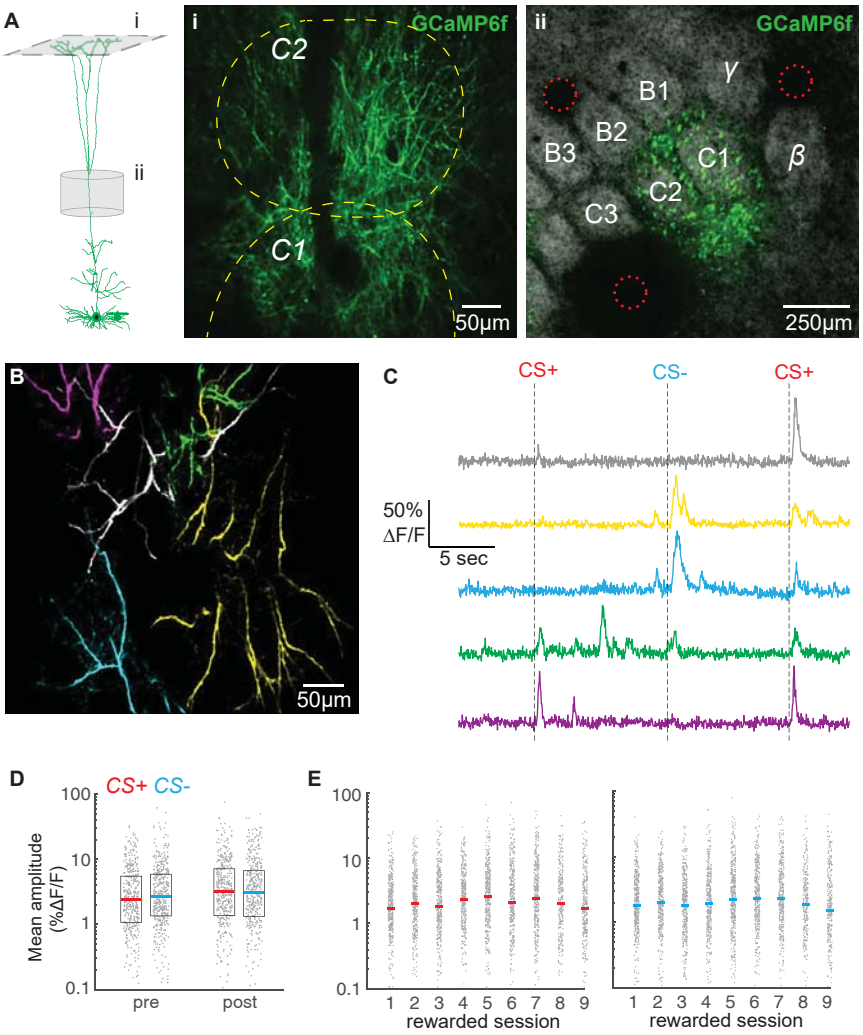
A
i
ii
i
GCaMP6f
C2
C1
50μm
ii
GCaMP6f
γ
B1
B2
B3
C1
β
C2
C3
250μm
B
50μm
C
CS+
CS-
CS+
50%
ΔF/F
5 sec
D
CS+ CS-
Mean amplitude (%ΔF/F)
100
10
1
0.1
pre
post
E
100
10
1
0.1
1 2 3 4 5 6 7 8 9
rewarded session
1 2 3 4 5 6 7 8 9
rewarded session

Figure 3

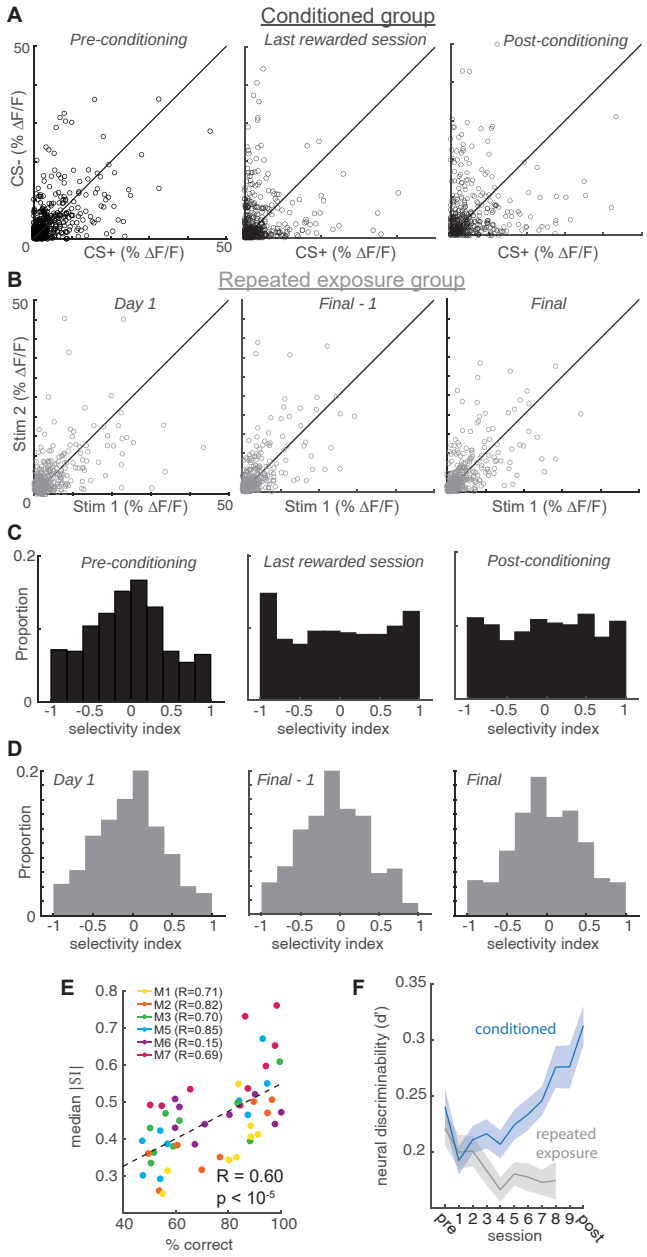
A
Conditioned group
Pre-conditioning
Last rewarded session
Post-conditioning
CS- (% ΔF/F)
CS+ (% ΔF/F)
B
Repeated exposure group
Day 1
Final - 1
Final
Stim 2 (% ΔF/F)
Stim 1 (% ΔF/F)
C
Proportion
selectivity index
D
E
M1 (R=0.71)
M2 (R=0.82)
M3 (R=0.70)
M5 (R=0.85)
M6 (R=0.15)
M7 (R=0.69)
median |SI|
% correct
R = 0.60
p < 10-5
F
neural discriminability (d')
conditioned
repeated exposure
pre
post
session

Figure 4

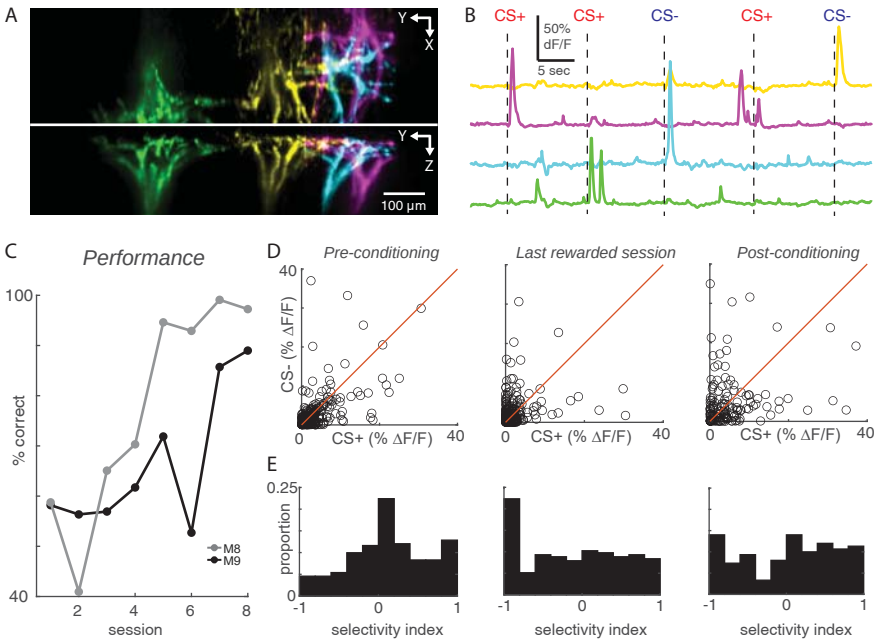
A
Y
X
Y
Z
100 µm
B
CS+
CS+
CS-
CS+
CS-
50% dF/F
5 sec
C
Performance
100
40
% correct
2
4
6
8
session
M8
M9
D
Pre-conditioning
Last rewarded session
Post-conditioning
40
CS- (% ΔF/F)
0
CS+ (% ΔF/F)
40
E
0.25
proportion
0
-1
0
1
selectivity index

Figure 5

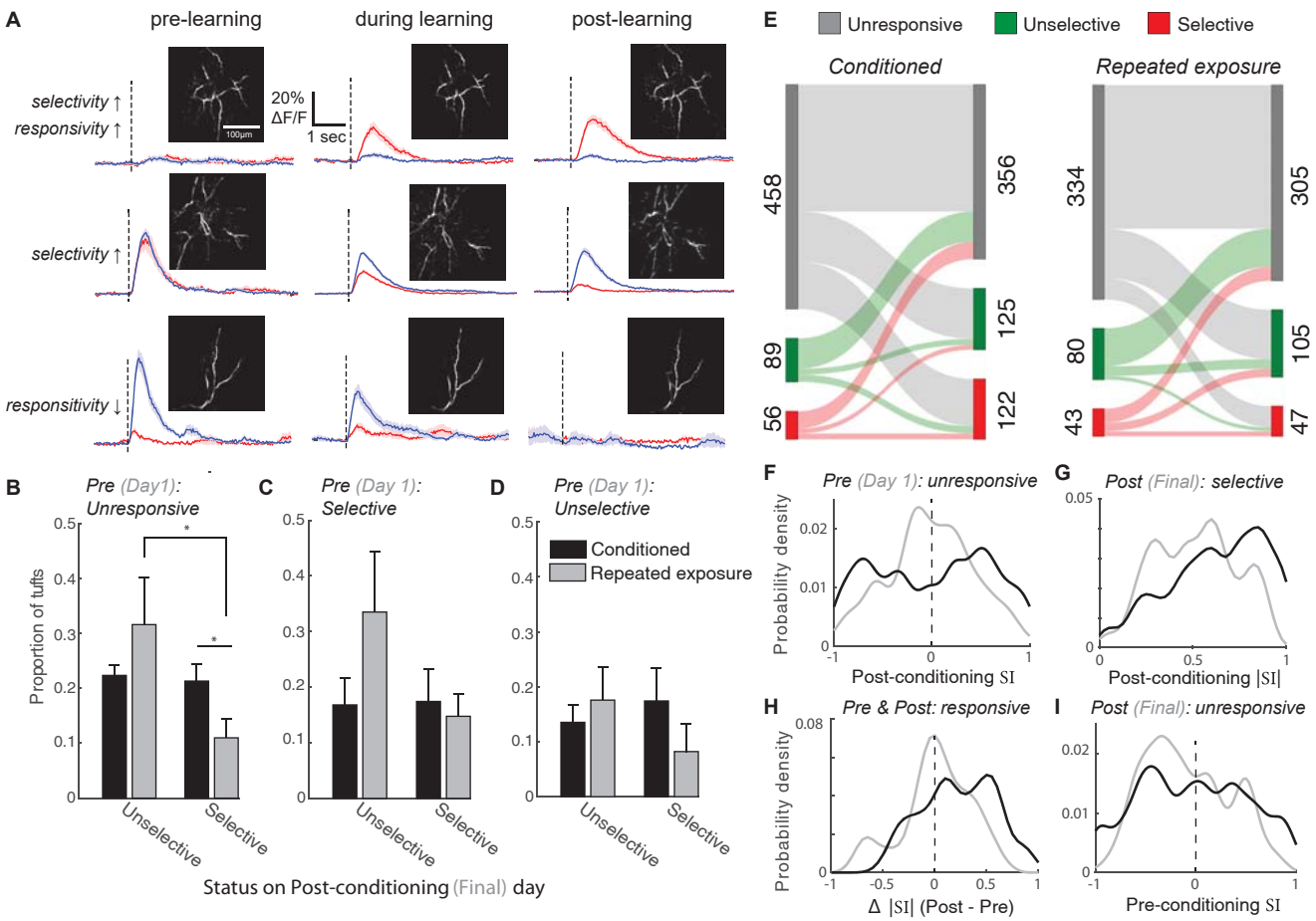
A
pre-learning
during learning
post-learning
selectivity ↑
responsivity ↑
selectivity ↑
responsivity ↓
20% ΔF/F
1 sec
100μm
B
Pre (Day1): Unresponsive
C
Pre (Day 1): Selective
D
Pre (Day 1): Unselective
Proportion of tufts
Conditioned
Repeated exposure
Unselective
Selective
Status on Post-conditioning (Final) day
E
Unresponsive
Unselective
Selective
Conditioned
Repeated exposure
458
89
56
356
125
122
334
80
43
305
105
47
F
Pre (Day 1): unresponsive
Probability density
Post-conditioning SI
G
Post (Final): selective
Post-conditioning |SI|
H
Pre & Post: responsive
Δ |SI| (Post - Pre)
I
Post (Final): unresponsive
Pre-conditioning SI

Figure 6

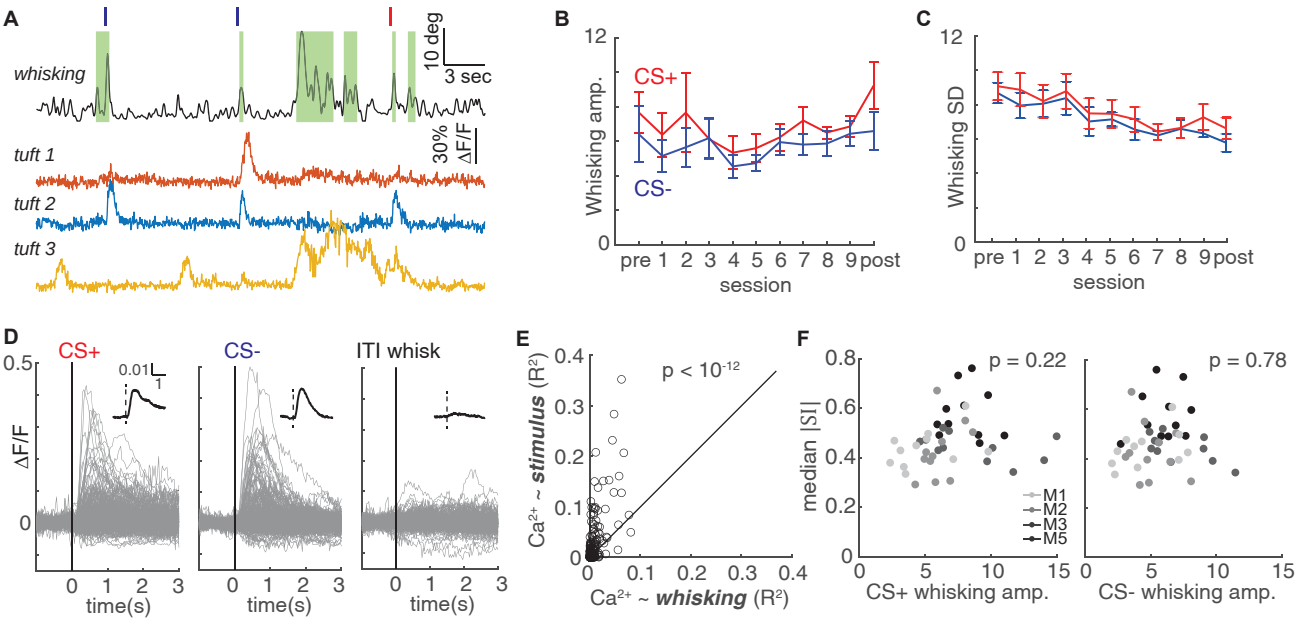
A
whisking
10 deg
3 sec
tuft 1
tuft 2
tuft 3
30% ΔF/F
B
CS+
CS-
Whisking amp.
12
0
pre 1 2 3 4 5 6 7 8 9 post
session
C
Whisking SD
12
0
pre 1 2 3 4 5 6 7 8 9 post
session
D
CS+
CS-
ITI whisk
ΔF/F
0.5
0
0.01
1
0 1 2 3
time(s)
E
p < 10-12
Ca2+ ~ stimulus (R2)
Ca2+ ~ whisking (R2)
0 0.1 0.2 0.3 0.4
F
p = 0.22
p = 0.78
median |SI|
0 0.2 0.4 0.6 0.8
M1
M2
M3
M5
0 5 10 15
CS+ whisking amp.
CS- whisking amp.

Figure 7

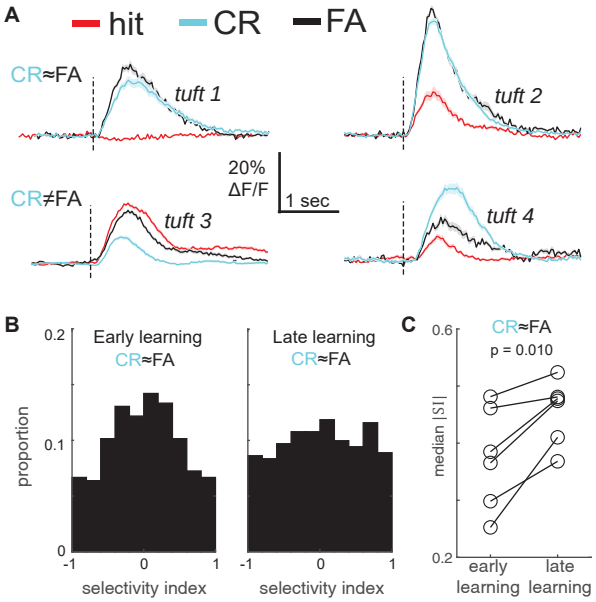
A
hit
CR
FA
CR≈FA
tuft 1
tuft 2
20%
ΔF/F
1 sec
CR≠FA
tuft 3
tuft 4
B
Early learning
CR≈FA
Late learning
CR≈FA
proportion
0.2
0.1
0
-1
0
1
selectivity index
C
CR≈FA
p = 0.010
median |SI|
0.6
0.2
early learning
late learning

Figure 8

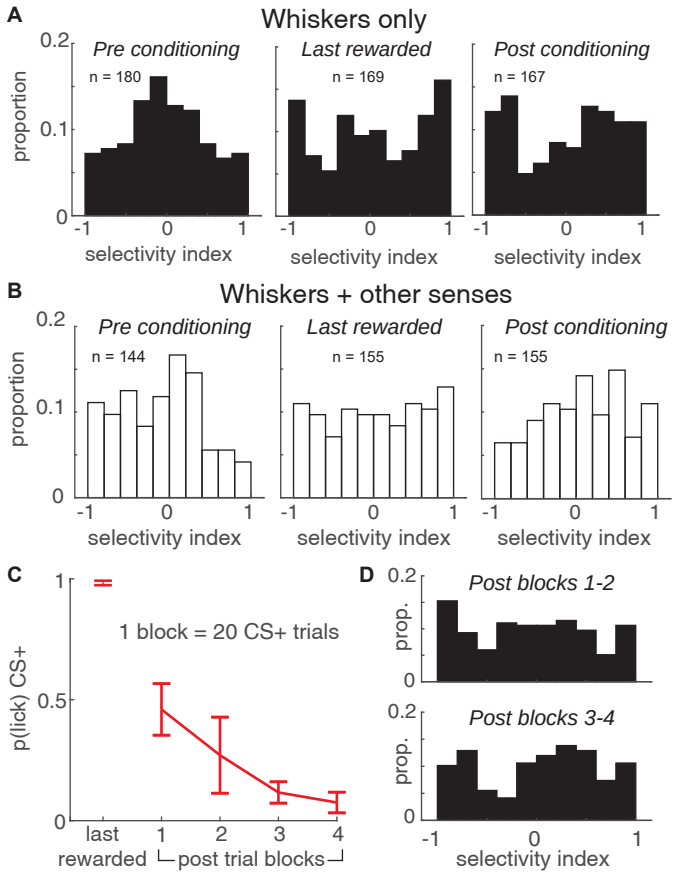
A
Whiskers only
Pre conditioning
Last rewarded
Post conditioning
n = 180
n = 169
n = 167
proportion
0.2
0.1
0
-1
0
1
selectivity index
B
Whiskers + other senses
n = 144
n = 155
n = 155
C
1
0.5
p(lick) CS+
1 block = 20 CS+ trials
last rewarded
2
3
4
post trial blocks
D
Post blocks 1-2
Post blocks 3-4
prop.

Supplementary Movie Legends

Supplementary Movie 1. Example two-photon microscopy movie during behavioral session.

Playback speed is in real time. “CS+” and “CS-” denote times of stimulus onset. 433 x 433 μm field of view.

Supplementary Movie 2. Example SCAPE microscopy movie during behavioral session. *Top*, maximum intensity projection (MIP) across the dorsal-ventral dimension showing horizontal extent of dendritic activity. *Bottom*, MIP across the medial-lateral dimension showing vertical extent of dendritic activity. Playback speed is in real time. “CS+” and “CS-” denote times of stimulus onset. 300 × 1050 × 234 μm field of view.

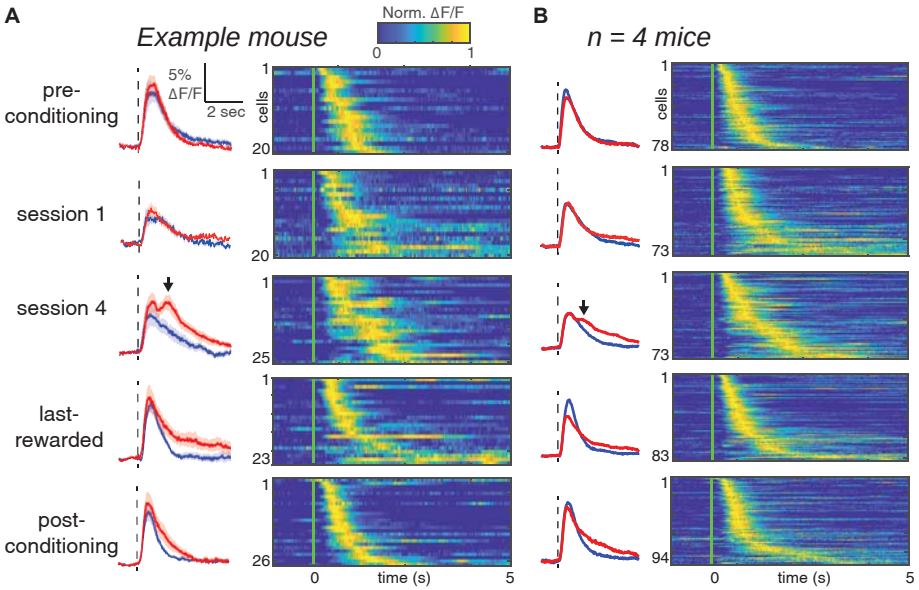

Supplementary Fig. 1 | CS+ trials evoke a second, long-latency peak during early learning, but not late learning. a, Left: Population average of stimulus-responsive tufts aligned to CS+ (red) or CS- (blue) trials from an example mouse. Right: Normalized ΔF/F of individual tufts during CS+ trials. **b**, Same as in a, combining data across four mice whose imaging regions were mapped with intrinsic imaging.

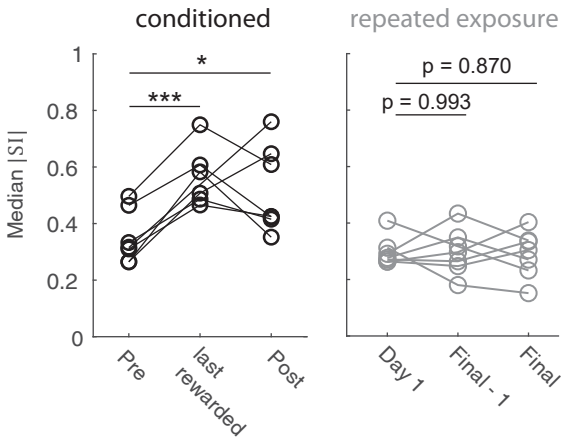

Supplementary Fig. 2 | Selectivity was enhanced in individual animals that received rewards. Median SI magnitude for each animal across three sessions for conditioned (left) and repeated exposure groups (right). * $p < 0.05$, *** $p < 10^{-3}$

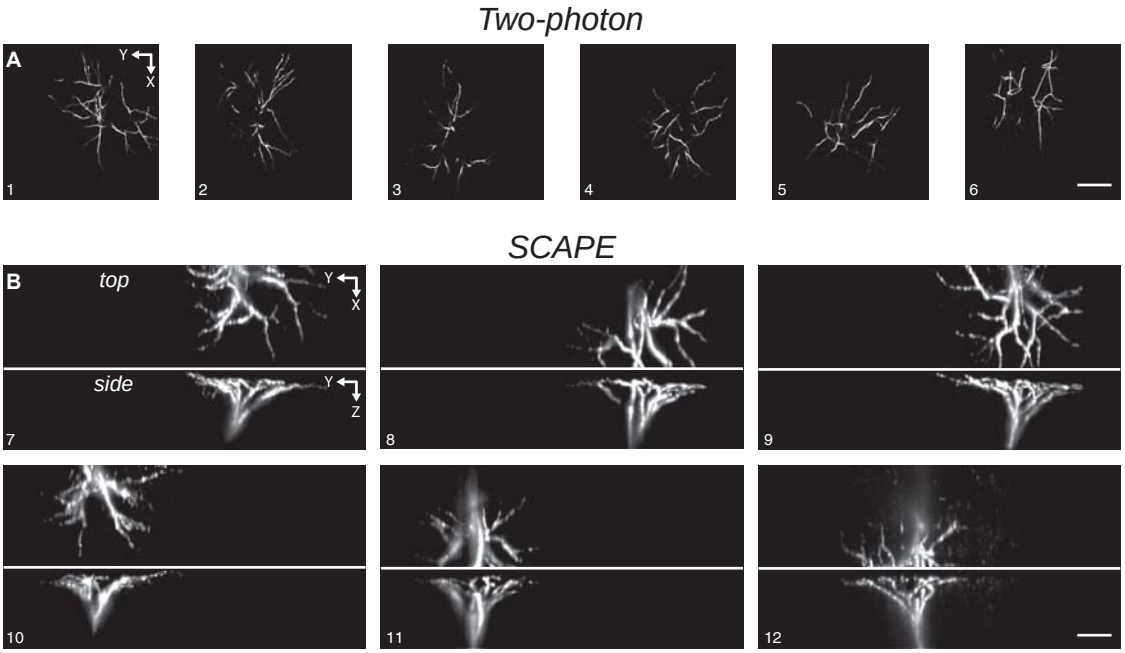

Supplementary Fig. 3 | Segmented tufts from two-photon and SCAPE microscopy. 12 example tufts extracted from either two-photon **(a)** or SCAPE microscopy **(b)**. Tufts segmented from SCAPE microscopy are shown as maximum intensity projections from the top and side. Scale bars: 100 µm.

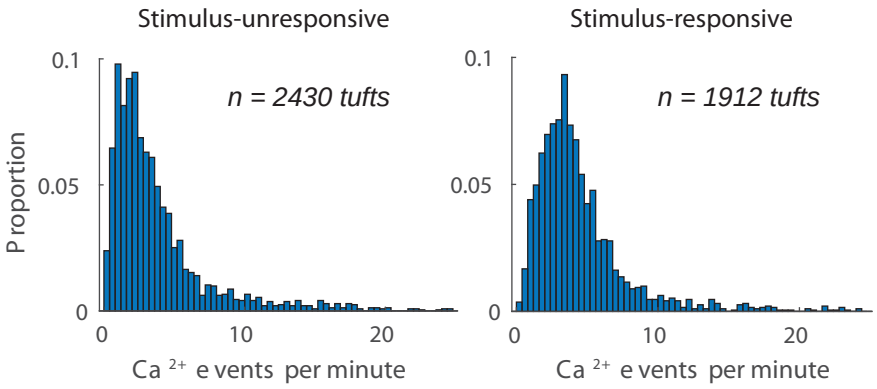

Supplementary Fig. 4 | Calcium event rate of tufts that were either unresponsive or responsive to air puff stimuli. The number of calcium events per minute was quantified for all tufts during each conditioning session. Data from each group was pooled across all sessions.

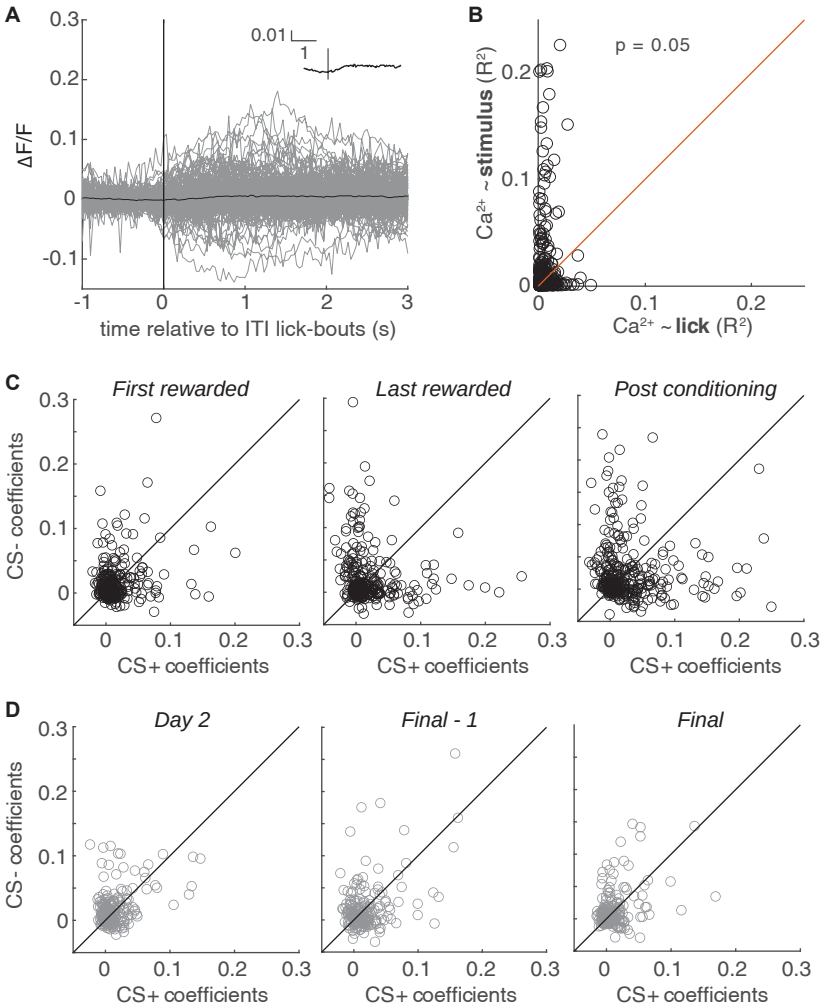

Supplementary Fig. 5 | Licking cannot account for changes in selectivity during learning. a, ITI lick-bout-triggered averages of 232 tufts on the 5th conditioning day, when ITI licks were still common (grey traces - individual tufts, black inset - population average), exhibit little or no lick-related calcium influx. **b**, R^2 values for linear models predicting calcium from stimuli (y axis) are consistently greater than those predicting calcium from licking (x axis). Each circle represents one tuft out of 442 tufts on last-rewarded sessions. **c**, Coefficients from a multivariate regression analysis with calcium as the response variable and the CS+, CS-, whisking, and licking as the predictors. CS+ and CS- coefficients are therefore disentangled from correlations with whisking and licking. Conditioning biases individual tufts (circles) to have larger CS+ or CS- coefficients. n = 304, 324, and 322 tufts for First rewarded, Last rewarded, and Post conditioning, respectively. **d**, Similar analysis to C but for repeated exposure group, with calcium as the response variable and the CS+, CS-, and whisking as the predictors. n = 223, 208, and 218 tufts for Day 2, Final - 1, and Final session, respectively.